Journal of Materials Chemistry A

ROYAL SOCIETY OF CHEMISTRY

REVIEW

View Article Online
View Journal | View Issue

Cite this: J. Mater. Chem. A, 2021, 9, 20874

Separation of alkane and alkene mixtures by metal–organic frameworks

Hao Wang, †[a] Dawei Luo,†[a] Ever Velasco,[b] Liang Yu[a] and Jing Li *[ba]

The separation of alkane/alkene gas mixtures represents an important yet challenging process in the petrochemical industry to produce valuable chemical feedstocks with sufficiently high purity. These molecules have similar physical properties, making their separation difficult and capital-intensive. The current separation and purification technology relies largely on heat-driven distillations with a huge unit composed of hundreds of trays. Adsorptive separation using porous solids is capable of accomplishing the purification under ambient conditions, offering potential energy and environmental benefits. In particular, metal–organic frameworks (MOFs) hold enormous promise for this separation process in light of their highly tunable pore shape, pore size, and pore surface functionality. In this review article, we provide a comprehensive account of metal–organic frameworks that have been investigated for the separation of alkanes and alkenes with a focus on C_2–C_3 hydrocarbons. The material design rationale, separation mechanisms, and structure–property relations are highlighted. Finally, the existing challenges and possible design strategies for desirable materials are also discussed.

Received 14th May 2021
Accepted 26th August 2021

DOI: 10.1039/d1ta04096k

rsc.li/materials-a

1. Introduction

The separation of light hydrocarbons into individual components with required purity remains an important goal in the petrochemical industry.[1,2] For example, with an annual global production of over 150 million metric tons, ethylene and propylene are among the most important feedstock for manufacturing various chemical commodities, including polyethylene and polypropylene. The prime feed of ethylene and propylene comes from refineries: either the by-products of steam cracking of naphtha, or off-gases from fluid catalytic cracking units. Olefins in these streams are accompanied by various impurities, in particular their corresponding alkanes, which must be removed to generate polymer-grade olefins as feedstock to produce valued polymers. The petrochemical industry currently relies on heat-driven distillations for these separations. To separate these physically similar molecules, the industry relies on huge distillation units with more than a hundred trays, which inevitably consumes tremendous amounts of energy. In this context, more economical technologies, such as adsorptive separation by porous solids or

[a]Hoffmann Institute of Advanced Materials, Shenzhen Polytechnic, 7098 Liuxian Blvd., Nanshan District, Shenzhen, Guangdong 518055, China
[b]Department of Chemistry and Chemical Biology, Rutgers University, 123 Bevier Road, Piscataway, NJ 08854, USA. E-mail: jingli@rutgers.edu
† These authors contributed equally to this work.

Hao Wang received his B.S. degree from Wuhan University, China, in 2012, and Ph.D. degree from Rutgers University, United States, in 2018. He then joined the Hoffmann Institute of Advanced Materials (HIAM) at Shenzhen Polytechnic, where he is currently an Associate Professor. His research focuses on the design of novel crystalline porous materials and their applications in industrially relevant separations.

Dawei Luo received his Ph.D. degree from the University of Science & Technology Beijing, China, in 2009. He then joined Shenzhen Polytechnic, where he is currently an Associate Professor. His research focuses on the design of novel nanomaterials and their applications in renewable energy.

membranes, are the focus of scientists and engineers in this field.

Adsorptive separation of alkane/alkene mixtures has been extensively investigated on traditional porous solids such as zeolites,[3,4] activated carbons,[5,6] and porous organic frameworks/polymers,[7–9] with zeolites as one of the most well developed classes. Various zeolites such as 13X, 4A, 5A, chabazite and ZK-5, to name a few, have been studied for the separation of propane/propylene or ethane/ethylene.[3,4,10–12] Zeolite 4A and silica chabazite (SiCHA) have been identified as the two most promising zeolite materials for the separation of propane and propylene.[12,13] Detailed adsorption/separation experiments and pressure vacuum swing adsorption (PVSA) processes have been carried out to evaluate their separation capability. While 4A requires lower separation energy per tonne of propylene compared to SiCHA, the low diffusivities limit its practical use. More recently, Corma *et al.* reported highly selective kinetic separation of ethane and ethylene by a flexible pure silica zeolite, ITQ-55.[3] Due to its structural flexibility, ITQ-55 exhibits much faster adsorption toward ethylene over ethane, with a kinetic selectivity of ~100. However, to date, no material has been widely employed for industrial alkane/alkene separation. An important factor that hinders their commercial application is a limited pool of ideal adsorbents with high adsorption capacity and selectivity that simultaneously possess stable structures and exhibit facile scale-up synthesis. The emergence and development of metal–organic frameworks (MOFs) over the past two decades has created a new opportunity for practical implementation of adsorptive separation of alkane/alkene mixtures under ambient conditions. MOFs hold particular promise for this separation process in light of their diverse structures, high surface area, and highly tunable pore structure (pore shape and pore size) and surface chemistry.[14–19] Tailored MOFs with an optimal structure and functionality and high separation efficiency may be achievable.

Hundreds of different MOFs have been investigated for the separation of alkane/alkene mixtures over the past few years, with a bunch of them outperforming traditional adsorbents with respect to separation efficiency (adsorption capacity and selectivity).[13,20,21] The separation mechanisms mainly include thermodynamic separation, kinetic separation, and selective molecular exclusion. Additionally, some materials show separations with a high dependence on temperature or pressure, originating from structural flexibility, which may not fall within the scope of the aforementioned three types of mechanism. MOFs that separate alkane/alkene mixtures *via* the thermodynamic mechanism can be alkene-selective or alkane-selective. Alkene-selective MOFs commonly contain Lewis acidic moieties such as open metal sites (OMSs) that provide strong interaction with π bonds of alkenes. Representative examples are the MOF-74 series. It is worth noting that alkane-selective MOF materials are advantageous over alkene-selective analogues in removing minor alkanes from alkenes; however, alkane-selective adsorbents were previously rare and have only recently seen an influx in various reports. This group of MOFs includes the well-known $Fe_2(O_2)$(dobdc) and the newly reported NIIC-20 family. Naturally, kinetic separation is observed when MOFs show different diffusional restrictions toward alkenes and their alkane counterparts. For example, a prototype material, ZIF-8, exhibits notable diffusional limitations for propane while propylene can enter its cages freely, leading to a propylene/propane kinetic selectivity of more than 100. Adsorbents with an optimal pore structure that are capable of

Ever Velasco received his B.S. degree from Rutgers University, United States in 2015. He is currently a graduate student in Professor Jing Li's research group at Rutgers University, United States. His research focuses mainly on the design and synthesis of MOFs for adsorptive separation of chemical species and the use of LMOFs for the luminescent sensing of toxic chemical species.

Liang Yu was a research assistant in the Hoffmann Institute of Advanced Materials (HIAM) at Shenzhen Polytechnic from 2018 to 2020. He is currently a first-year doctoral student in the School of Chemistry and Chemical Engineering of South China University of Technology. His research focuses on the design and preparation of novel metal–organic frameworks and their applications in gas separation.

Jing Li received her Ph.D. degree from Cornell University in 1990 under the guidance of Professor Roald Hoffmann. She joined the chemistry faculty at Rutgers University in 1991 as an Assistant Professor. She was promoted to Associate Professor in 1996, to Full Professor in 1999, and to Distinguished Professor in 2006. Her research focuses on designing and developing new and functional materials (including MOFs and hybrid semiconductors) for renewable, sustainable, and clean energy related applications.

full separation of alkane/alkene mixtures through selective molecular exclusion are desirable for industrial implementation as such a mechanism provides infinite selectivity and high separation efficiency. This has been rarely observed for zeolites resulting from the lack of structural tunability. However, several tailor-made MOFs have achieved the separation of propane/propylene through selective molecular exclusion, including KAUST-7, Y-abtc, and Co-gallate. Such precise control of the pore aperture can be attributed to the high structural tunability of MOFs and the power of reticular chemistry.

In this review article, we attempt to provide a comprehensive account of the MOFs reported to date that show potential for adsorptive separation of C_2–C_3 alkane/alkene mixtures. Adsorption capacity and selectivity for these materials under ambient conditions are summarized. The compositions of alkane/alkene mixtures depend on the feed and the preceding cracking processes. Equimolar mixtures are typically used for research purposes. Ideal adsorbed solution theory (IAST) has been widely used to predict the adsorption selectivity of an adsorbent and is also summarized in this work. In most studies, experimental multicomponent column breakthrough measurements were carried out to evaluate the separation capability of the adsorbents. In addition, we focus particularly on the underlying adsorption/separation mechanism and design strategy for tailored MOF adsorbents (Scheme 1).

2. Thermodynamic separation

Thermodynamically driven separation is commonly observed for MOFs and other adsorbents. This occurs when the pore size of an adsorbent is large enough to accommodate all adsorbates.

Each of these individual adsorbates experiences an adsorbate–adsorbent interaction that results in preferential adsorption of adsorbates with stronger adsorption affinity. Alkene-selective adsorbents are more common in traditional inorganic and organic adsorbents, as well as in MOFs. However, a number of MOFs showing alkane-selective behavior have been developed over the past few years (Table 1).

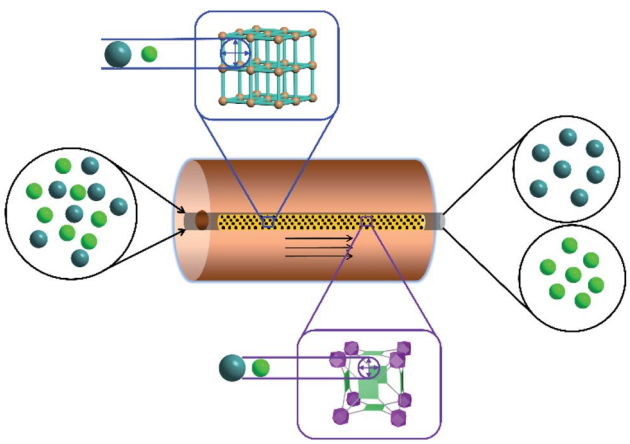

Scheme 1 Schematic illustration of adsorptive separation by MOFs.

2.1 Alkene-selective separation

It has been well demonstrated that MOFs with OMSs preferentially interact with unsaturated hydrocarbons over their saturated counterparts, resulting in thermodynamic separation of alkane/alkene mixtures. They behave in a similar fashion to the previously known π-complexation adsorbents.

The first MOF with OMSs studied for alkane/alkene separation is the prototype Cu–BTC (HKUST-1, H_3BTC = 1,3,5-benzenetricarboxylic acid). Bhatia *et al.* conducted quantum mechanical calculations using a Cu–tricarboxylate complex portion of Cu–BTC and investigated its adsorption toward ethylene and ethane.[22,23] The results indicated that at low loadings ethylene was favored as a result of its strong electrostatic interactions with the framework, leading to an ethylene/ethane selectivity of 2. However, the selective adsorption was weakened at higher loadings due to the stronger van der Waals affinity of ethane with the complex. In a subsequent study, Wang *et al.* performed Grand Canonical Monte Carlo (GCMC) simulations of adsorption and separation of ethylene/ethane mixtures on Cu–BTC.[24] The ethylene/ethane selectivity was calculated to be 2, which is consistent with the previous results. Nevertheless, no decrease of selectivity with an increase in pressure was observed in this GCMC calculation. Experimental evaluation of alkane/alkene separation by Cu–BTC was carried out by Limia *et al.* and Yoon *et al.* Preferential adsorption of propylene over propane was observed with higher adsorption capacity and isosteric heat.[25] Very recently, Wu *et al.* developed a functionalized Cu–BTC material, $Pyr_{1/3}$@Cu–BTC, by grafting pyrrole molecules onto the open Cu sites of the framework.[26] The separation capability of propylene and propane by this material was evaluated and compared to that of its parent structure. The results suggested that the functionalized MOF shows enhanced adsorption capacity and selectivity. $Pyr_{1/3}$@Cu–BTC exhibited a notably high adsorption capacity of 7.6 mmol g^{-1} for propylene at 298 K and 1 bar, higher than that of the pristine Cu–BTC (7.0 mmol g^{-1}). In addition, an increase of IAST propylene/propane selectivity from 4.1 to 5.5 for an equimolar binary mixture was observed upon pyrrole functionalization. Its capability for the separation of propane and propylene was confirmed by multicomponent column breakthrough measurements. More importantly, the grafted pyrrole molecules protected the Cu sites from being attacking by H_2O, leading to largely enhanced moisture stability of the functionalized material. This study indicated that judicious functionalization on OMSs of a MOF with optimal loading may simultaneously enhance its olefin/paraffin separation efficiency and structural stability towards water.

Another MOF with OMSs that was examined for alkane/alkene separation at the early stage of this research field was MIL-100(Fe). The study was carried out by Serre *et al.* in 2010.[27] MIL-100(Fe) is built on μ_3-oxo-centered trimers of Fe^{III} octahedra where two out of three iron octahedra have terminal H_2O molecules that can be removed upon heating leading to the exposure of open Fe^{III} sites (activation at 100 °C) or a mixture of Fe^{II} and Fe^{III} sites (activation at 250 °C). Adsorption measurements of propane and propylene were performed on both

samples (activated at 100 °C and 250 °C) and the results indicated that the presence of Fe^{II} dramatically enhanced the adsorption affinity toward propylene and propylene/propane selectivity at low pressure. Open Fe^{III} sites are also effective in the preferential adsorption of propylene over propane; however, their interaction with propylene is weakened compared to that of Fe^{II}. The authors attributed this to the presence of an additional d electron in the iron(II) orbitals leading to a π back-bonding interaction with propylene. The feasibility of using MIL-100(Fe) for the separation of propane and propylene was confirmed by breakthrough tests with equimolar propane/propylene binary mixtures. Their results show that a column packed with a 250 °C activated sample can elute propane out at the 7th minute while propylene was retained in the column for 175 minutes, indicating a clear separation between the two gases. A propylene/propane separation factor of 28.9 was calculated from the breakthrough results at low pressure. This value was substantially higher than that for Cu–BTC in previous studies. However, a pronounced decrease in the separation factor was observed with increasing partial pressure of the gas mixture resulting from the involvement of Fe^{III}.

The MOF-74-M (M = Zn, Fe, Co, Ni, Mn, Mg, *etc.*) family represents the most extensively studied materials in this category. This family of materials can be easily synthesized through solvothermal reactions with H_4DOBDC (2,5-dihydroxyterephthalic acid) and the corresponding metal nitrate in a DMF–ethanol–water mixed solvent with relatively high yield. Bao *et al.* carried out the first study of alkane/alkene separation with materials in this family.[29] With combined experimental exploration and GCMC simulation, the authors investigated the adsorption and separation of ethane, ethylene, propane, and propylene on MOF-74-Mg. As expected, the compound showed favoured adsorption toward propylene and ethylene over propane and ethane, with higher adsorption capacity and stronger affinity for the former. GCMC simulation revealed that all four adsorbate molecules are preferentially adsorbed on the open Mg sites but with stronger interaction for alkenes. It is noteworthy that the material demonstrated higher adsorption affinity to propylene and propane than to ethane and ethylene, which should be attributed to the significant dipole moments of the former. In an independent study carried out almost at the same time, Bae *et al.* evaluated the performance of MOF-74-M (M = Co, Mn, and Mg) for the separation of propane and propylene.[28] All three compounds showed selective adsorption of propylene over propane, as evidenced by single-component gas adsorption experiments and multicomponent column breakthrough measurements (Fig. 1). However, propylene/propane selectivity was found to be highly dependent on metal species in this series of MOFs, and the values followed the order of Co > Mn > Mg. MOF-74-Co showed an IAST selectivity of 46 for an equimolar binary mixture at 298 K and 1 bar, notably higher than that of MIL-100(Fe), the previous record holder. The underlying reason was explored by first-principles calculations for the binding energies between propylene/propane and all three compounds. It was revealed that MOF-74-Co had the highest binding energy towards propylene compared to the other two analogues. Additionally, it also showed the largest difference between binding energies for propylene and propane leading to the highest propylene/propane selectivity. Interestingly, different trends of alkene/alkane selectivity as a function of pressure were observed by the authors for MOF-74-Co. The selectivity of propylene/propane increased as pressure increased while for ethylene/ethane the trend was reversed. The authors attributed this to the proper match of the pore size and the size of propane/propylene molecules, leading to competitive adsorption between propane and propylene onto the OMSs as pressure increased. In contrast, a considerable pore volume was left for the adsorption of additional ethane or ethylene after the OMSs were occupied mainly by ethylene molecules and thus ethylene/ethane selectivity decreased as pressure increased.

In another study reported simultaneously, Long *et al.* carried out an in-depth investigation of alkane/alkene adsorption and separation on MOF-74-Fe,[30] which has a higher surface area and softer metal character compared to its analogues in previous studies (Fig. 2). Single-component adsorption results indicated that the uptake amounts of ethylene and propylene were approaching one molecule per iron(II) center at 313 K and 1 bar, while the adsorbed amounts of ethane and propane were notably lower, particularly at the low pressure region. Neutron powder diffraction analysis confirmed that open iron(II) centers in the structure of MOF-74-Fe were the primary binding sites for alkenes. Ethylene and propylene interact with iron(II) through side-on binding modes, with Fe–C distances of 2.42 and 2.56 Å, respectively. Column breakthrough measurements displayed that the material was capable of separating ethylene/ethane and propylene/propane mixtures into individual components with 99%+ purity. IAST adsorption selectivity of ethylene/ethane for MOF-74-Fe was calculated to be 13 to 18 at 318 K, higher than that of zeolite NaX and its isostructural Mg analogue as a result of the softer character of Fe(II) relative to Mg(II), leading to a stronger interaction between alkene molecules and the former. To further evaluate the alkene/alkane separation capability of MOF-74-Fe and compare it with that of other adsorbents, the authors carried out simulated breakthrough modelling. The amount of polymer-grade (99.5%+) propylene that can be produced was calculated from simulated breakthrough curves for MOF-74-Fe and a series of reported materials. The results indicated that MOF-74-Fe showed a higher propylene/propane separation efficiency than that of all other zeolites and MOFs, including ITQ-12, NaX, Cu–BTC, Cr–BTC, MIL-100-Fe, and MOF-74-Mg. This should be attributed to the fact that MOF-74-Fe has both high alkene/alkane selectivity and high adsorption capacity. Evaluation for ethylene/ethane mixtures also indicates that MOF-74-Fe outperformed other adsorbents studied.

In a subsequent study, Long *et al.* performed a systematic evaluation of alkane/alkene separation for the entire series of MOF-74-M (M = Mg, Mn, Fe, Co, Ni, Zn).[31] The adsorption capacity and selectivity of these materials is closely related to the metal species. IAST calculations from experimental isotherms indicated that MOF-74-Fe and MOF-74-Mn had the highest selectivities for ethylene/ethane and propylene/propane, respectively. In contrast, the Mg and Zn analogues exhibited the lowest selectivities for both separations, which

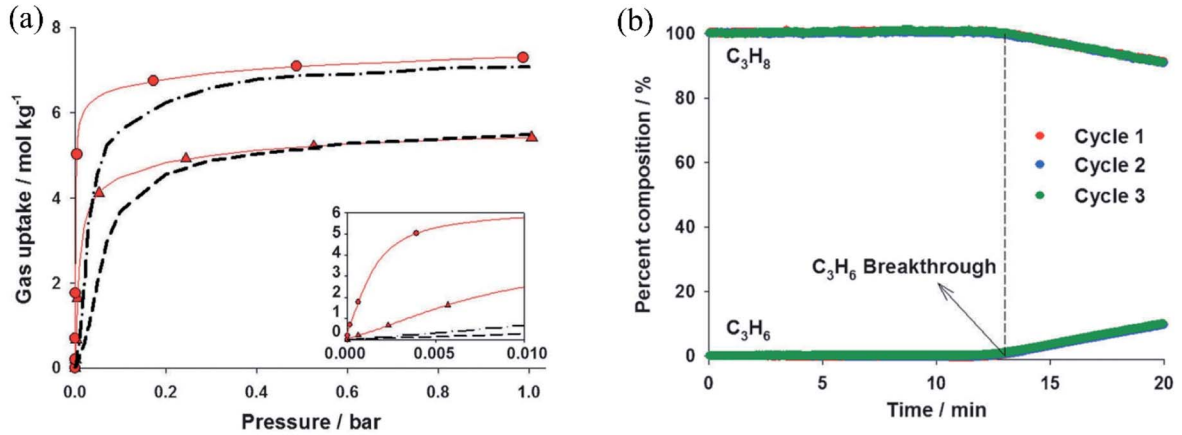

Fig. 1 (a) Adsorption isotherms for C_3H_6 (circles) and C_3H_8 (triangles) in Co-MOF-74 at 298 K. The inset shows the low-pressure isotherms. Solid lines through the experimental data are fits of the dual-site Langmuir–Freundlich model. (b) Breakthrough curves of equimolar mixtures of propene and propane (total flow rate = 30 mL min^{-1}) in a packed column of Co-MOF-74 that is initially saturated with C_3H_8. These curves were obtained for three consecutive cycles after the column had been regenerated by flowing pure propane. Reproduced with permission.[28] Copyright 2012, Wiley-VCH.

was attributed to the weaker affinities of these metals to olefins. This was confirmed by the isosteric heats of adsorption (Q_{st}) where MOF-74-Fe and MOF-74-Mn had the highest value for ethylene and propylene, respectively, while the Mg and Zn analogues showed the lowest value for the two olefins.

Inspired by the excellent performance of MOF-74-M (M_2(*p*-dobdc)) for the separation of alkane/alkene mixtures, Long *et al.* developed a new series of MOFs built on *m*-dobdc in order to alter the affinity of the OMSs and their olefin/paraffin selectivities.[32] The new materials can be prepared in the gram scale by stirring a mixture of H_4(*m*-dobdc) and the corresponding metal chloride in DMF under heating. The formed M_2(*m*-dobdc) (M = Mg, Mn, Fe, Co, Ni) feature isostructures to MOF-74-M. Experimental results indicated that M_2(*m*-dobdc) exhibited markedly

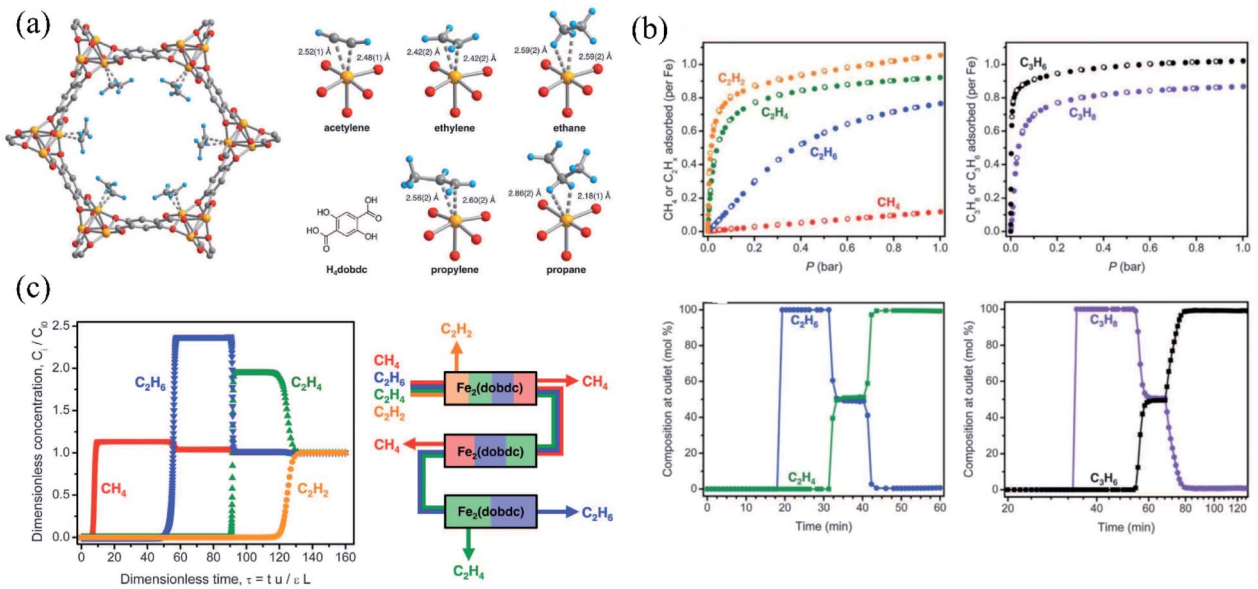

Fig. 2 (a) (Left) A portion of the solid-state structure of Fe_2(dobdc)·$2C_2D_4$ as determined by analysis of neutron powder diffraction data; orange, red, gray, and blue spheres represent Fe, O, C, and D atoms, respectively. (Right) H_4(dobdc) ligand and the first coordination spheres for the iron centers in the solid-state structures obtained upon dosing Fe_2(dobdc) with acetylene, ethylene, ethane, propylene, and propane. (b) (Top) Gas adsorption isotherms for methane, ethane, ethylene, and acetylene as well as propane and propylene in Fe_2(dobdc) at 318 K. Filled and open circles represent adsorption and desorption data, respectively. (Bottom) Experimental breakthrough curves for the adsorption of equimolar ethane/ethylene and propane/propylene mixtures flowing through a 1.5 mL bed of Fe_2(dobdc) at 318 K with a total gas flow of 2 mL min^{-1} at atmospheric pressure. (c) (Left) Calculated methane (red), ethane (blue), ethylene (green), and acetylene (orange) breakthrough curves for an equimolar mixture of the gases at 1 bar flowing through a fixed bed of Fe_2(dobdc) at 318 K. (Right) Schematic representation of the separation of a mixture of methane, ethane, ethylene, and acetylene using just three packed beds of Fe_2(dobdc) in a vacuum swing adsorption or temperature swing adsorption process. Reproduced with permission.[30] Copyright 2012, AAAS.

enhanced alkene/alkane selectivities compared to their *para*-functionalized counterparts (Fig. 3). In particular, Fe_2(*m*-dobdc) showed ethylene/ethane and propylene/propane selectivities of 25 and 55, respectively. This was attributed to the higher charge density at the metal sites in the *meta*-substituted variants leading to stronger adsorption affinity to alkenes compared to their *para*-substituted isomers. The hypothesis was experimentally confirmed by *in situ* single-crystal X-ray diffraction analysis of ethylene adsorbed crystals which showed a shorter Co–C distance in Co_2(*m*-dobdc) than that in Fe_2(*p*-dobdc). The selective adsorption of alkenes over alkanes on M_2(*m*-dobdc) resulted from the preferential adsorption of alkene molecules on OMSs, similar to that for M_2(*p*-dobdc). Expected side-on interactions between alkenes and OMSs in M_2(*m*-dobdc) were also experimentally observed. The combined features of high adsorption capacity and selectivity, fast adsorption kinetics, and relatively low cost make M_2(*m*-dobdc) promising adsorbents for alkene/alkane separations. The authors concluded that the material design strategy employed in this work may be generalized and that tuning the electronic environment around a given adsorption site in a given structure may largely affect adsorption and separation properties.

Besides OMSs formed intrinsically in MOF structures, metal binding sites which are added post-synthetically to the materials may also play an important role in favoured adsorption of alkenes over alkanes. Bao *et al.* reported the immobilization of Ag(I) into sulfonic acid functionalized MIL-101(Cr) to form MIL-101(Cr)–SO_3Ag.[33] MIL-101(Cr)–SO_3Ag was easily obtained by stirring a mixture of MIL-101(Cr)–SO_3H and $AgBF_4$ in a mixed solvent of CH_3CN/H_2O. The Ag(I) loaded compound showed a suppressed BET surface area of 1253 $m^2\ g^{-1}$ compared to that of the pristine MIL-101(Cr)–SO_3H (1856 $m^2\ g^{-1}$). However, the adsorption capacities of ethylene and propylene were noticeably enhanced upon Ag(I) loading particularly at the low pressure region indicating strong interactions between Ag(I) and alkene molecules. This was confirmed by the isosteric heats of adsorption results. The Q_{st} values of ethylene and propylene in MIL-101(Cr)–SO_3H were 35 and 41 kJ mol^{-1} while the values for MIL-101(Cr)–SO_3Ag were calculated to be 120 and 101 kJ mol^{-1}, which are comparable to the binding energies in Ag(I)-based π-complexation systems. This indicated that the substantially enhanced affinity toward alkenes in MIL-101(Cr)–SO_3Ag should originate from the π-complexation between alkene molecules and the loaded Ag(I) ions. The enhanced interactions with alkenes in MIL-101(Cr)–SO_3Ag led to its notably improved alkene/alkane selectivity. The IAST selectivity of ethylene/ethane increased from 1.15 for MIL-101(Cr)–SO_3H to 16 for its Ag(I) loaded analogue. A similar strategy was also effectively applied to other adsorbents such as porous aromatic frameworks.[9]

In a more recent study,[34] Qian *et al.* developed Cu^I@UiO-66–$(COOH)_2$ with an optimal pore window size and chelated Cu(I) ions that forms π-complexation with ethylene (Fig. 4). The loading of Cu(I) was carefully carried out in a glovebox under an inert atmosphere by stirring CuCl and the parent material in acetonitrile. The authors systematically investigated the evolution of surface area, pore size, and ethylene/ethane separation properties from UiO-66–COOH and UiO-66–$(COOH)_2$ to Cu^I@UiO-66–(COOH) and Cu^I@UiO-66–$(COOH)_2$. The loading

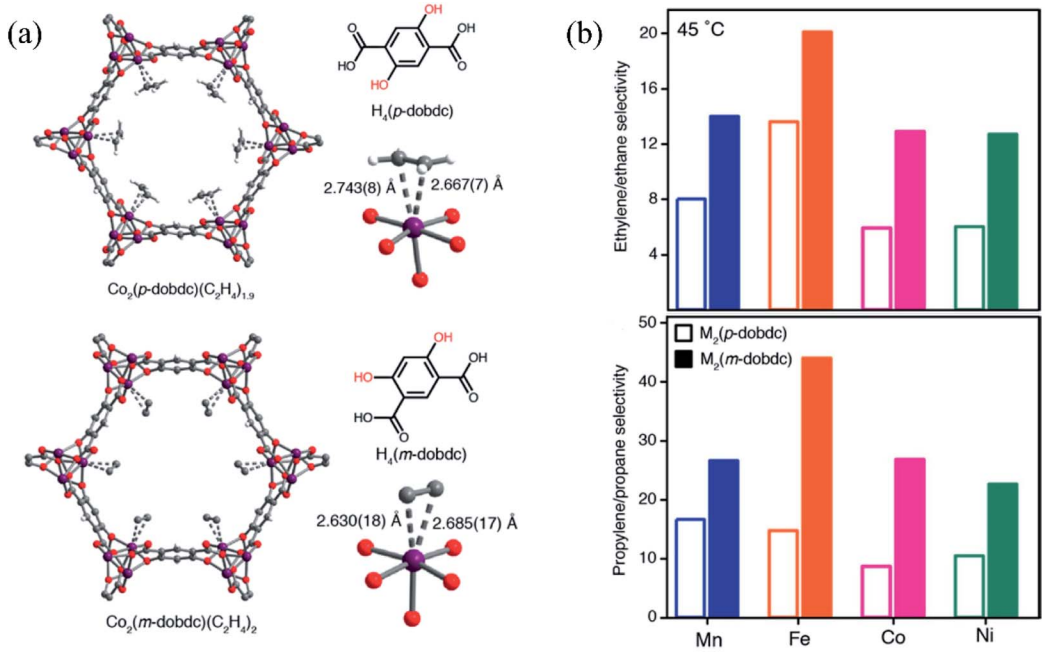

Fig. 3 (a) Comparison of the framework structures, ligand structure, and ethylene binding geometries for (top) Co_2(*p*-dobdc) and (bottom) Co_2(*m*-dobdc) under ~0.3 bar of ethylene at 100 K as determined from *in situ* single-crystal X-ray diffraction experiments. Purple, red, gray, and white spheres represent Co, O, C, and H atoms, respectively. (b) Comparison of the IAST selectivity under an equimolar feed at 45 °C between M_2(*p*-dobdc) and M_2(*m*-dobdc) (M = Mn, Fe, Co, Ni) for (top) ethylene/ethane and (bottom) propylene/propane separations. Reproduced with permission.[32] Copyright 2017, American Chemical Society.

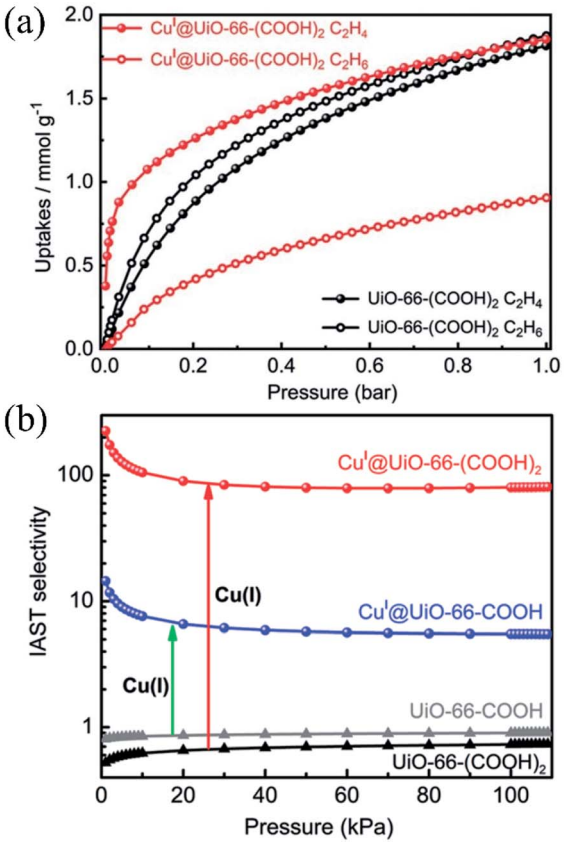

Fig. 4 (a) Single-component adsorption isotherms for C_2H_4 and C_2H_6 of UiO-66-(COOH)$_2$ and Cu^{I}@UiO-66-(COOH)$_2$ at 298 K. (b) IAST calculations of activated UiO-66-type MOFs for the C_2H_4/C_2H_6 separation at 298 K. Reproduced with permission.[34] Copyright 2020, Wiley-VCH.

of –COOH functional groups and Cu(I) ions not only offers strong adsorption sites for ethylene, but also tunes the pore aperture so that ethylene is optimally adsorbed while ethane is partially excluded in Cu^{I}@UiO-66-(COOH)$_2$. This led to an exceptionally high ethylene/ethane selectivity of 80.8 in Cu^{I}@UiO-66-(COOH)$_2$, outperforming most previously described benchmark adsorbents.

MOFs without OMSs or additional metal binding sites may also be capable of selectively adsorbing alkenes over alkanes through soft supramolecular interactions. The representative MOF in this category is NOTT-300 reported by Yang *et al.*[36] NOTT-300 is built on one-dimensional (1D) [$AlO_4(OH)_2$] chains bridged by biphenyl-3,3′,5,5′-tetracarboxylate (bptc^{4-}) linkers affording a three-dimensional (3D) porous structure possessing 1D channels with a diameter of 6.5 Å. The compound has a BET surface area of 1370 m^2 g^{-1}. It adsorbed 4.28 mmol g^{-1} of ethylene at 293 K and 1 bar, which was substantially higher than that for ethane (0.85 mmol g^{-1}) under identical conditions. The great difference in the uptakes between ethylene and ethane in NOTT-300 led to a remarkably high ethylene/ethane selectivity of 48.7, exceeding the values for adsorbents reported prior to this work. Combined exploration by *in situ* synchrotron X-ray and neutron powder diffraction, inelastic neutron scattering (INS), and DFT calculations revealed that ethylene exhibited a side-on interaction with the HO–Al group *via* hydrogen bonding and π⋯π stacking interactions with the phenyl rings. In comparison, the adsorbed ethane molecules were aligned at a very long distance to the –OH groups because of an absence of π-electron density and repulsion between the hydrogen atoms, leading to its weaker interaction with the framework compared to ethylene. This study indicated that the relatively weak supramolecular bonding interactions in MOFs may be sufficiently strong to selectively adsorb alkenes over alkanes with high adsorption selectivity.

Anion-pillared MOFs have been extensively studied for the separation of alkyne/alkene as well as alkene/alkane mixtures. Cui *et al.* reported the separation of propylene and propane by two isostructural anion-pillared MOFs, GeFSIX-2-Cu-i and SIFSIX-2-Cu-i (Fig. 5).[35] Both materials showed selective adsorption of propylene over propane, originating from the strong hydrogen-bonding interactions between GeF_6^{2-}/SiF_6^{2-} anions and propylene in addition to π–π interactions between the organic linkers and C_3H_6. The extent of adsorption affinity was characterized by isosteric heats of adsorption. GeFSIX-2-Cu-

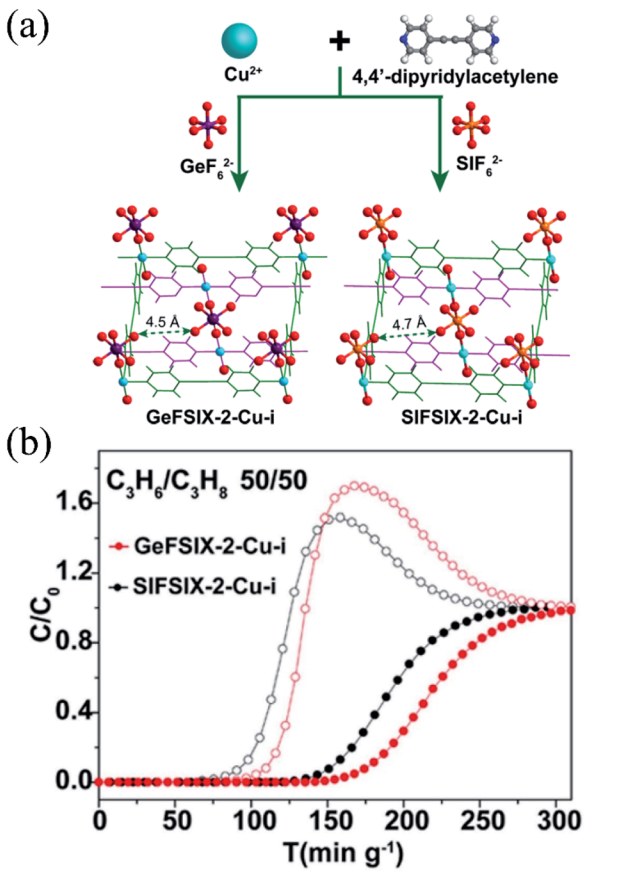

Fig. 5 (a) Structures of GeFSIX-2-Cu-i and SIFSIX-2-Cu-i. Color code: F, red; N, blue; Cu, indigo; Ge, purple; Si, yellow; H, light gray; C, green/rose red (the different nets are highlighted in green and rose red for clarity). (b) Breakthrough tests for C_3H_6/C_3H_8 (50/50, v/v) at 298 K and 1 bar carried out on GeFSIX-2-Cu-i and SIFSIX-2-Cu-i. Reproduced with permission.[35] Copyright 2020, American Chemical Society.

Table 1 Representative MOFs showing thermodynamic separation for alkane/alkene mixtures[a]

	MOF	BET surface area ($m^2\ g^{-1}$)	Aperture size (Å)	Uptake (mmol g^{-1}) alkene	alkane	Selec.	Temp. (K)	Ref.
C_3H_8/C_3H_6	Propylene-selective							
	MOF-74-Fe	1536	11	6.9	6.2	14.7	318	39
	MOF-74-Mg	1835	11	7.5	6.0	5.5	318	29, 31
	MOF-74-Mn	1797	11	7.2	6.0	16.6	318	31
	MOF-74-Co	1438	11	6.8	5.9	8.6	318	31
	MOF-74-Ni	1532	11	7.0	5.7	10.4	318	31
	MOF-74-Zn	1277	11	6.3	5.5	3.9	318	31
	MIL-101-Cr–SO_3H	1856	15	4.5	3.8	1.1	303	33
	MIL-101(Cr)–SO_3H–Ag	1253	15	4.3	3.0	6.0	303	33
	ZIF-4	300	4.9	2.4	2.4	1.1	293	40
	Mn_2(*m*-dobdc)	—	—	7.5	6.0	40	298	32
	Fe_2(*m*-dobdc)	—	—	7.5	6.0	52	298	32
	Co_2(*m*-dobdc)	—	—	7.5	6.0	39	298	32
	Ni_2(*m*-dobdc)	—	—	7.5	6.0	35	298	32
	Cu@MIL-100(Fe)	1490	5.5	3.4	2.2	34	323	41
	Zn_2(5-aip)$_2$(bpy)	—	8.1	1.9	0.7	20	298	42
	NJU-Bai8	1048	—	2.8	2.8	4	298	37
	MIL-101(Cr)–DAA	3501	—	7.5	6.5	2	303	43
	AGTU-3a	227	—	1.2	0.5	7	298	44
	GeFSIX-2-Cu-i	—	4.5	2.7	1.6	4.0	298	35
	$Pyr_{1/3}$@Cu–BTC	1510	8.5	7.0	6.7	5.5	298	26
	Propane-selective							
	WOFOUR-1-Ni	—	5.6	1.2	1.0	1.6	298	45
	BUT-10	1726	—	6.3	5.8	1.4	298	46
	Zr–BPDC	2094	11	8.8	8.4	1.2	298	47
	g-C_3N_4@Zr–BPDC	2409	11	8.9	8.9	1.4	298	47
	Zr–BPYDC	2080	12	6.8	7.2	1.6	298	47
	ZIF-8	1844	3.4	4.5	4.6	1.3	298	48
C_2H_6/C_2H_4	Ethylene-selective							
	MOF-74-Fe	1536	11	6.3	5.2	13.6	318	30, 31
	MOF-74-Mg	1835	11	6.2	4.8	4.4	318	29, 31
	MOF-74-Mn	1797	11	6.3	5.2	8.1	318	31
	MOF-74-Co	1438	11	6.2	5.3	5.8	318	31
	MOF-74-Ni	1532	11	6.0	4.7	5.9	318	31
	MOF-74-Zn	1277	11	5.4	4.6	2.7	318	31
	MIL-101-Cr–SO_3H	1856	15	1.7	1.6	1.2	303	33
	MIL-101-Cr–SO_3H–Ag	1253	15	2.6	1.2	16	303	33
	ZIF-4	300	4.9	2.3	2.2	2.0	293	40
	Mn_2(*m*-dobdc)	—	—	6.8	6.1	17	298	32
	Fe_2(*m*-dobdc)	—	—	7.0	6.2	25	298	32
	Co_2(*m*-dobdc)	—	—	7.0	6.2	15	298	32
	Ni_2(*m*-dobdc)	—	—	6.6	6.0	16	298	32
	MIL-101	2892	—	4.0	2.9	0.8	303	49
	MIL-101-6Cu	1680	—	4.5	2.0	12.5	303	49
	MIL-101-6Ni	2110	—	4.3	2.4	1.2	303	49
	CPL-2	—	—	2.9	2.8	1.5	298	50
	Ag/CPL-2	—	—	0.9	0.2	25	298	50
	1.6AgM-DS	846	—	3.4	1.0	9.5	298	51
	Cu^I@UiO-66–COOH	437	4.5	1.4	0.9	5.5	298	34
	Cu^I@UiO-66–$(COOH)_2$	319	4.1	1.9	0.9	80.8	298	34
	NUS-36	298	3.5	1.5	1.0	4.1	298	52
	Ca(squarate)	224	3.4	2.3	1.3	5.9	298	53
	NUS-6(Hf)–Ag	1027	—	2.0	1.3	6.0	298	54
	Ethane-selective							
	DUT-8(Cu)	2370	—	1.9	3.4	1.4	303	55
	DUT-8(Ni)	2440	—	2.3	4.0	1.7	303	55
	CPM-80-Zn	995	13.3	4.2	4.7	1.8	298	56
	CPM-80-Co	895	13.3	3.8	4.2	1.8	298	56
	CPM-80-Fe	862	13.3	4.0	4.5	1.8	298	56
	CPM-81-Zn	907	13.3	4.1	4.4	1.8	298	56

Table 1 (*Contd.*)

MOF	BET surface area ($m^2\ g^{-1}$)	Aperture size (Å)	Uptake ($mmol\ g^{-1}$) alkene	alkane	Selec.	Temp. (K)	Ref.
CPM-81-Co	1020	13.3	5.1	5.4	1.8	298	56
CPM-82-Zn	568	13.3	3.5	4.0	1.6	298	56
NIIC-20-Et	1161	~25	1.8	2.4	3.5	298	57
NIIC-20-Pr	1117	~25	1.9	2.4	4.0	298	57
NIIC-20-Bu	1033	~25	1.4	2.5	15.4	298	57
NIIC-20-Pe	1023	~25	1.6	2.2	8.4	298	57
NIIC-20-GI	963	~25	1.7	2.1	8.7	298	57
MUF-15	1130	3.6	4.1	4.6	2.0	293	58, 59
MUF-15-F	874	3.4	2.9	3.2	1.1	293	58
MUF-15-Br	734	3.3	2.1	2.0	1.3	293	58
MUF-15-NO_2	762	—	2.7	2.5	0.4	293	58
MUF-15-CH_3	967	3.5	2.6	2.7	1.6	293	58
Ca(H_2tcpb)	200	5.5	2.7	2.8	2.0	298	60
Ni1-a	1474	5.5	5.2	5.9	1.6	298	61
CPM-63m	1023	—	2.5	2.9	1.5	298	62
Y–BTC	933	—	3.1	3.5	1.9	298	63
Sm–BTC	700	—	1.6	1.7	1.8	298	63
Eu–BTC	720	—	2.8	3.1	1.9	298	63
Dy–BTC	947	—	1.9	1.9	1.4	298	63
Mn–PNMI	818	13.3	2.0	2.7	1.4	298	64
Zn–PNMI	305	—	1.5	1.6	1.4	298	64
Cd–PNMI	264	—	1.4	1.9	1.3	298	64
$Cu(Qc)_2$	240	—	2.0	0.8	3.4	298	65, 66
RT-$Cu(Qc)_2$	251	—	0.6	2.2	4.1	298	65
NUM-7a	345	3.4	2.7	2.9	1.7	298	67
NJU-120	1597	4.4	3.9	4.9	2.7	296	68
Cr–BTC(O_2)	1135	—	2.9	3.3	1.5	298	69
CPM-733	1328	7.3	6.3	7.1	1.7	298	70
CPM-736	472	5.9	3.9	4.0	1.6	298	70
CPM-738	1161	5.9	4.6	4.7	1.4	298	70
CPM-723	1369	6.8	6.7	6.9	1.5	298	70
CPM-223(Ti)	1460	6.8	6.3	6.9	1.6	298	70
CPM-223-tppy	1599	6.8	7.3	7.2	1.3	298	70
CPM-223-tpbz	1661	6.8	6.2	6.9	1.5	298	70
CPM-223(V)	1597	6.8	6.5	7.4	1.6	298	70
Ni(bdc)$(ted)_{0.5}$	1905	5.8	3.3	4.8	1.6	298	71, 72
Zn(bdc)$(ted)_{0.5}$	1781	5.8	3.2	4.5	1.5	298	71
Co(bdc)$(ted)_{0.5}$	1708	5.8	2.8	4.1	1.6	298	71
Cu(bdc)$(ted)_{0.5}$*b*	1631	5.9	2.5	3.7	1.6	298	71
JNU-2	1219	3.7	3.5	4.1	—	298	73
Zr–bptc	1085	5.0	3.1	3.3	1.4	298	74
UiO-66-2CF_3	467	—	1.5	1.8	2.3	298	75
Ni-4PyC	945	5.0	3.5	3.8	1.7	298	76
Ni(BDC)$(DABCO)_{0.5}$	2050	8.6	3.1	4.3	1.6	298	77
Ni$(BDC)_{0.8}(TMBDC)_{0.2}(DABCO)_{0.5}$	1556	8.0	4.0	4.9	1.7	298	77
Ni$(BDC)_{0.55}(TMBDC)_{0.45}(DABCO)_{0.5}$	1294	8.0	4.3	5.0	1.7	298	77
Ni$(BDC)_{0.29}(TMBDC)_{0.71}(DABCO)_{0.5}$	1084	7.3	4.8	5.5	1.9	298	77
Ni(TMBDC)$(DABCO)_{0.5}$	894	5.9	5.0	5.4	2.0	298	77
In-soc-MOF-1	1223	6.8	3.7	4.0	1.4	298	78
UiO-66-ADC	556	4.4	1.7	1.6	1.8	298	52
MIL-53(Al)-FA	1160	6.0	3.8	3.9	1.8	298	60
$Fe_2(O_2)$(dobdc)	1073	—	2.5	3.3	4.4	298	20
MIL-142A	1555	10	2.9	3.8	1.5	298	79
PCN-245	1743	10	2.4	3.3	1.8	298	80
PCN-250	1470	5.9	4.2	5.2	1.8	298	81
ZIF-69	882	—	1.8	2.2	1.7	298	82
MAF-49	—	—	1.7	1.7	2.7	316	83
IRMOF-8	1360	12.6	3.1	4.1	1.8	298	84

[a] Notes: (1) gas uptakes were measured at the specified temperature and 1 bar. (2) Selectivities were calculated using the IAST model.

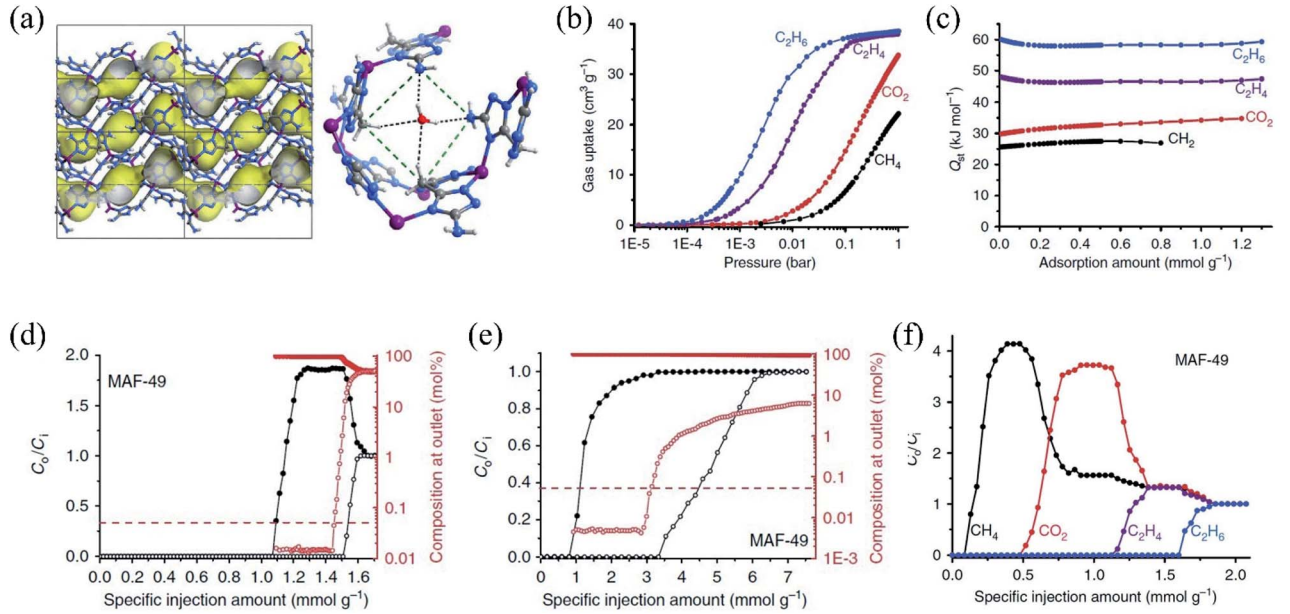

Fig. 6 (a) X-ray crystal structure of MAF-49·H_2O. (b) Gas adsorption isotherms for C_2H_6, C_2H_4, CO_2 and CH_4 in MAF-49 at 316 K. (c) Coverage-dependent C_2H_6, C_2H_4, CO_2 and CH_4 adsorption enthalpy obtained by the Virial method. (d) C_2H_4/C_2H_6 (1 : 1) mixture breakthrough curves of MAF-49. (e) C_2H_4/C_2H_6 (15 : 1) mixture breakthrough curves of MAF-49. (f) Breakthrough curves of a $CH_4/CO_2/C_2H_4/C_2H_6$ mixture (1 : 1 : 1 : 1 (vol)) for MAF-49 measured at 313 K and 1 bar. Reproduced with permission.[93] Copyright 2015, Springer Nature.

i showed a Q_{st} of 35.8 kJ mol^{-1} for propylene, notably higher than that for propane (20.4 kJ mol^{-1}). It is noteworthy that these values are lower compared to those of MOFs with OMSs or other stronger adsorption sites and may be beneficial for material regeneration in practical applications.

Flexible MOFs represent a unique family of materials that usually show unexpected adsorption behaviors toward various guest molecules. This can sometimes be beneficial for applications relating to gas storage and separation. Structural flexibility of MOFs may be selectively utilized for the separation of alkene/alkane mixtures. Since structural transformations of MOFs relate to the extent of host–guest interactions, we will discuss these within the thermodynamically driven separation category. Li *et al.* reported the separation of propane and propylene in a flexible MOF, NJU-Bai8, through its guest-dependent, pressure induced gate-opening effect.[37] NIU-Bai8 is built on paddle-wheel $Cu_2(COO)_4N_2$ SBUs bridged by 5-(pyrimidin-5-yl)isophthalate linkers forming a 3D structure with 1D channels. The dumbbell-like channels are decorated with bulging pyrimidine rings that swell upon guest inclusion and removal, thus resulting in structural flexibility. The adsorption profiles of propylene and propane were characterized by "S" shaped curves which are commonly observed for flexible MOFs. There is essentially no uptake before gate-opening pressure while after the threshold pressure the adsorption rapidly reaches saturation. For a given temperature, the gate-opening pressure for propylene is notably lower than that of propane, indicating stronger interaction between the former and the framework. The difference in gate-opening pressures for propylene and propane can be utilized for the separation of these two gases, and the feasibility was confirmed by experimental column breakthrough measurements.

With synergistic sorbent separation technology (SSST), Zaworotko *et al.* achieved one-step ethylene purification from a four-component mixture including ethylene, ethane, acetylene, and carbon dioxide.[38] A series of different adsorbents were packed in a single column to enhance the separation efficiency for multicomponent gas mixtures. For example, a three-component sorbent bed was used to separate a four-component equimolar mixture of $C_2H_2/C_2H_4/C_2H_6/CO_2$. Column breakthrough measurements indicated that CO_2, C_2H_6, and C_2H_2 were preferentially captured so that C_2H_4 eluted out with polymer-grade purity. The SSST strategy may be generalized and the adsorbents can be optimized to achieve highly selective separation toward specific gas mixtures.

2.2 Alkane-selective separation

Most of the reported porous materials for alkene/alkane separation, including zeolites, metal oxides, and MOFs, show alkene-favored behavior. This could be attributed to the stronger interaction between alkene molecules and metal centers/clusters through π-complexation. We have also presented in the foregoing examples that without metal binding sites MOFs may also show selective adsorption of alkenes over alkanes through supramolecular interactions such as π···π stacking. However, since alkenes are the favored components in alkene/alkane separation, an additional desorption step is needed if alkene-selective adsorbents are employed. In comparison, alkane-selective adsorbents would be more desirable, particularly in the cases where minor alkane impurities need to be removed from alkenes, as they produce high-purity

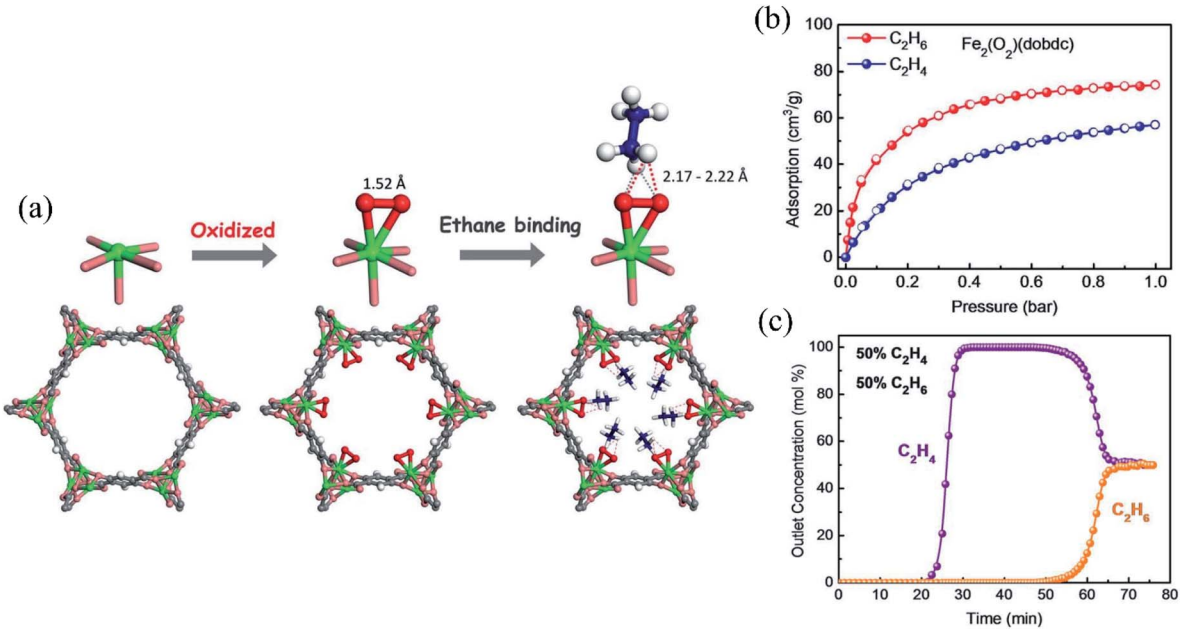

Fig. 7 (a) Structures determined from NPD studies. Shown are structures of Fe_2(dobdc), $Fe_2(O_2)$(dobdc), and $Fe_2(O_2)$dobdc$\supset C_2D_6$ at 7 K. (b) Adsorption (solid) and desorption (open) isotherms of C_2H_6 (red circles) and C_2H_4 (blue circles) in $Fe_2(O_2)$(dobdc) at 298 K. (c) Experimental column breakthrough curves for a C_2H_6/C_2H_4 (50/50) mixture in an absorber bed packed with $Fe_2(O_2)$(dobdc) at 298 K and 1.01 bar. Reproduced with permission.[20] Copyright 2018, AAAS.

alkenes directly during the adsorption step. This would make the separation scheme much simpler and efficient. It has been proposed that nonpolar/inert surfaces such as aromatic or aliphatic moieties are important features for alkane-selective adsorbents. A number of MOFs which selectively adsorb alkanes over alkenes have been reported over the past few years.

Gascon *et al.* reported a very early study on alkane-selective alkane/alkene separation by a flexible MOF, ZIF-7.[85] ZIF-7 is built on Zn(II) and benzimidazole linkers, with a pore aperture of about 3 Å for the activated structure. However, as a result of the structural flexibility, it may accommodate guest molecules larger than 3 Å into its cages, characterized by the gate-opening step in the adsorption isotherms. Single-component adsorption measurements revealed that the threshold pressure for ethane was much lower than that for ethylene. As observed for other flexible MOFs, gate-opening pressure relates to the interaction between the adsorbate and the organic linker at the pore window of ZIF-7. The difference in the threshold pressure of ethane and ethylene created a pressure window where ethane is adsorbed while ethylene is not. For the first time, the authors experimentally confirmed that the material was ethane-selective for a binary ethane/ethylene mixture through column breakthrough measurements. It is noteworthy that even though the partial pressure of ethylene in the mixture is higher than its gate-opening pressure in ZIF-7, a remarkable ethane/ethylene selectivity was observed. In a subsequent study,[84] Pires *et al.* explored the ethane-selective behavior of IRMOF-8. IRMOF-8 is built on Zn(II) and naphthalene-2,6-dicarboxylate and is isoreticular to MOF-5. Single-component adsorption isotherms at 298 K up to 10 bar revealed that the material favored ethane over ethylene and was confirmed by column breakthrough experiments using ethylene/ethane binary mixtures as the feed. Density functional theory (DFT) calculations indicated that the contributions from the two adjacent rings in the MOF structure result in a higher interaction energy for ethane than that of ethylene. The authors concluded that MOFs with organic linkers with high aromaticity are prone to be ethane-selective materials.

An important study in the early explorations for MOFs that preferentially adsorb alkanes over alkenes was carried out by Zhang *et al.* on MAF-49 (Fig. 6).[83] Different from the previously reported alkane-selective MOFs which generally possessed a low-polarity or hydrophobic pore surface, MAF-49 featured rather polar pore functionality. The compound was constructed from Zn(II) and bis((5-amino-1*H*-1,2,4-triazol-3-yl)methane) (H_2batz) as the organic linker, synthesized solvothermally in aqueous ammonia solution. The ligand was designed to have multiple nitrogen atoms as hydrogen-bonding acceptors and methylene groups as dipole repulsion groups. MAF-49 possesses 1D zigzag channels with the narrowest section of 3.3 × 3.0 Å, and multiple electronegative, uncoordinated nitrogen atoms at the pore surface that may be involved in hydrogen bonding. Single-component adsorption isotherms at 316 K revealed that ethane is notably favored at low pressure compared to ethylene although the saturation uptakes at 1 bar are similar for the two gases. Heats of adsorption calculations indicated that the Q_{st} for ethane is 60 kJ mol^{-1}, higher than that for ethylene (48 kJ mol^{-1}). The relatively high adsorption affinity of ethane suggested that multiple supramolecular interactions may exist between ethane and the framework. This was confirmed by GCMC simulation and further periodic DFT optimization of the host–guest structures. Ethane interacted

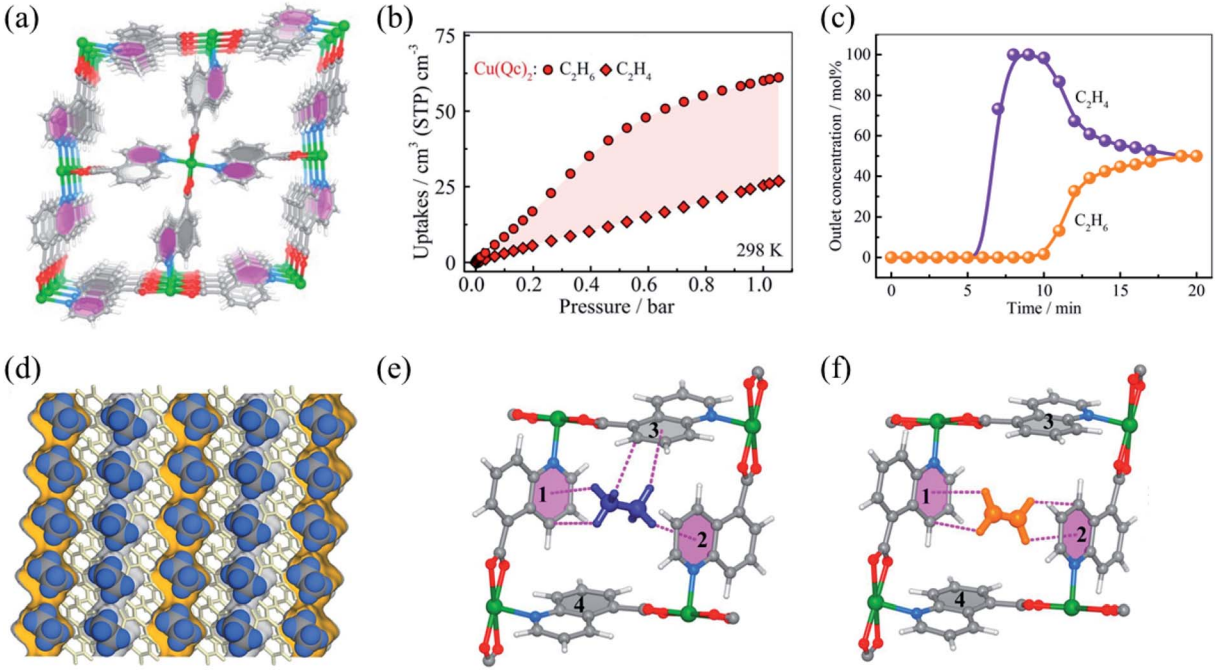

Fig. 8 (a) Crystal structure of $Cu(Qc)_2$. (b) C_2H_6 and C_2H_4 sorption isotherms for $Cu(Qc)_2$ at 298 K. (c) Experimental column breakthrough curves for an equimolar C_2H_6/C_2H_4 (orange/purple) mixture (298 K, 1 bar) in an adsorber bed packed with $Cu(Qc)_2$. (d and e) Neutron diffraction crystal structures of ethane loaded $Cu(Qc)_2$. (f) Neutron diffraction crystal structures of ethylene loaded $Cu(Qc)_2$. Reproduced with permission.[66] Copyright 2018, American Chemical Society.

with the pore surface of MAF-49 through multiple strong C–H···N hydrogen bonds and weak electrostatic interactions while for ethylene the extent of these interactions was much weaker. The feasibility of ethane/ethylene separation by MAF-49 was evaluated by column breakthrough measurements using a binary mixture of 15 : 1 ethylene/ethane as a feed, mimicking industrial mixtures produced by hydrocarbon cracking. It was revealed that ethylene with a purity of 99.995% can be obtained through a single breakthrough step with an ethylene productivity of 1.68 mmol g^{-1} (99.95%+ purity). This was much more efficient than previously reported ethane-selective MOFs such as IR-MOF-8 and MAF-4 under identical conditions. This study indicated that ethane-selective MOFs may be achievable by rational utilization of polar functional groups and optimization of the surface electrostatic distribution that may result in stronger binding to ethane over ethylene.

Li *et al.* demonstrated the exceptional ethane-selective ethane/ethylene separation by $Fe_2(O_2)$dobdc in 2018 (Fig. 7).[20] The material, $Fe_2(O_2)$dobdc, was developed by Long *et al.* early in 2011 through the oxidation of solvent-free Fe_2(dobdc) by oxygen.[86] $Fe_2(O_2)$dobdc retains the crystal structure of its parent compound Fe_2(dobdc) upon functionalization, but is characterized by the iron(III)-peroxo sites on its pore surface. In contrast to the pristine MOF Fe_2(dobdc) which favors ethylene over ethane, $Fe_2(O_2)$dobdc shows a notable preference to ethane. It adsorbed 3.3 mmol g^{-1} of ethane at 298 K and 1 bar, noticeably higher than that of ethylene (2.5 mmol g^{-1}) under identical conditions. Ethane showed a Q_{st} of 66.8 kJ mol^{-1}, higher than that of other ethane-selective MOFs including the previously illustrated MAF-49, indicating the strong interaction between ethane and the framework. The gas–MOF interaction was uncovered by neutron powder diffraction (NPD) measurements. It was revealed that ethane molecules preferentially interacted with the peroxo sites through C–H···O hydrogen bonds. DFT calculations further confirmed the preferential binding sites suggested by NPD, indicating that the ethane/ethylene adsorption selectivity was a result of the peroxo active sites and the electronegative surface oxygen distribution in $Fe_2(O_2)$dobdc. Remarkably, $Fe_2(O_2)$dobdc exhibited an ethane/ethylene IAST selectivity of 4.4 at 298 K and 1 bar, outperforming previously reported ethane-selective MOFs such as MAF-49 and IR-MOF-8. The authors carried out systematic column breakthrough measurements with different multicomponent feeds, demonstrating the capability of $Fe_2(O_2)$dobdc for the separation of ethane and ethylene. It is noteworthy that the authors in this work not only demonstrated a distinct MOF material for highly efficient separation of ethane and ethylene through ethane-selective adsorption, but also developed a general approach for immobilizing strong adsorption sites to produce alkane-selective adsorbents. The material design strategy has been successfully employed in Cr–BTC and Cu–BTC.[69] Both Cr–BTC(O_2) and Cu–BTC(O_2) showed selective adsorption of ethane over ethylene, while the adsorption preferences were reversed in their parent structures. However, it is noteworthy that the reported MOFs with metal-peroxo sites are sensitive to moisture and all the measurements were performed under an inert atmosphere.

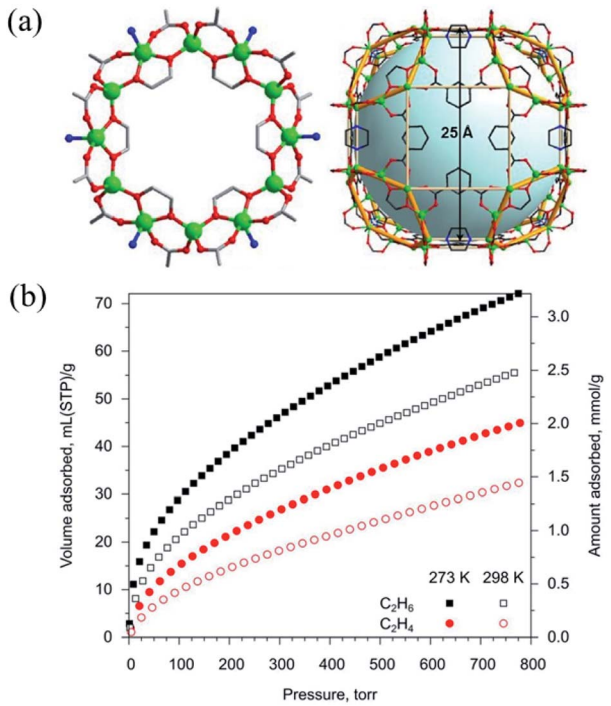

Fig. 9 (a) Crystal structure of NIIC-20-Et. (b) The adsorption isotherms of C_2H_6 and C_2H_4 at 273 K (filled symbols) and 298 K (empty symbols) for NIIC-20-Bu. Reproduced with permission.[57] Copyright 2020, Wiley VCH.

A surge in the number of reported ethane-selective MOFs since 2018 has been observed. A variety of material design/functionalization strategies have been applied and several studies focusing on computational screening or mechanistic exploration have also been presented. Pinto *et al.* reported the enhancement of ethane/ethylene adsorption selectivity by the introduction of perfluoro groups in Zr-MOFs.[75] Compared to UiO-66 (Zr-BDC), Zr-NDC, and UiO-66-Br which showed almost identical adsorption toward ethane and ethylene, UiO-66-2CF_3 exhibited a preference for ethane over ethylene. The IAST ethane/ethylene adsorption selectivity for UiO-66-2CF_3 was calculated to be 2.5. The selectivity was retained at higher pressures up to 1000 kPa. Computational explorations revealed the possibly stronger interaction between the organic linker and ethane than ethylene. This work demonstrated that the introduction of bulky CF_3 groups may be more efficient for the improvement of ethane/ethylene selectivity in MOFs than increasing the aromaticity of the organic linker.

Chen *et al.* reported the improvement of ethane/ethylene selectivity by controlling the pore structures in isoreticular, ultramicroporous MOFs.[66] The authors investigated the adsorption and separation of ethane and ethylene on $Cu(ina)_2$ (Hina = isonicotinic acid) and $Cu(Qc)_2$ (HQc = quinolone-5-carboxylic acid), two microporous structures with the same connectivity but different pore sizes. $Cu(Qc)_2$ has a pore aperture of 3.3 Å in its activated form, smaller than that of $Cu(ina)_2$ (4.1 Å). $Cu(ina)_2$ exhibited slightly higher adsorption capacity for ethane over ethylene. However, the ethane-selective adsorption behavior was much more distinct in $Cu(Qc)_2$ (Fig. 8). It adsorbed 1.85 mmol g^{-1} of ethane at 298 K and 1 bar, substantially higher than that of ethylene (0.78 mmol g^{-1}). The IAST ethane/ethylene selectivity was calculated to be 3.4 at 298 K and 1 bar for $Cu(Qc)_2$. This value was higher than those of most of the previously reported ethane-selective adsorbents. Column breakthrough measurements of an equimolar ethane/ethylene mixture revealed that the material was capable of separating ethane and ethylene. The resulting ethylene that eluted was detected to have 99.9%+ purity at the outlet before the breakthrough of ethane. The underlying mechanism of favored adsorption of ethane over ethylene by $Cu(Qc)_2$ was explored through neutron powder diffraction studies. The results indicated that the cavity of $Cu(Qc)_2$ was optimal for the accommodation of ethane which enabled the binding for ethane molecules through multiple C–H$\cdots\pi$ interactions. In comparison, the resulting interactions between ethylene molecules and the cavities result in lower binding affinity. The authors concluded that an applicable design strategy to produce ethane-selective MOFs with high efficiency would include increasing the efficient contact area or the number of specific interactions between the pore surface and ethane. More recently,[65] Tang *et al.* reported the facile synthesis of $Cu(Qc)_2$ by stirring at room temperature to produce a highly crystalline phase within 1 hour. The material prepared at room temperature (denoted as RT-$Cu(Qc)_2$) showed higher ethane uptake and lower ethylene uptake at 298 K at 1 bar, resulting in a higher ethane/ethylene uptake ratio and selectivity. The IAST ethane/ethylene selectivity for RT-$Cu(Qc)_2$ was 4.1, outperforming most of the previously reported ethane-selective MOFs. Nevertheless, it was not clear why the $Cu(Qc)_2$ synthesized at room temperature performed better than the one prepared from solvothermal reactions.

Feng *et al.* developed a series of ethane-selective MOFs with high ethane uptake through the pore space partition (PSP) strategy.[70] The materials were built on a MIL-88 type framework by introducing a pore partitioning agent into its hexagonal channel, with a resultant formula of $[(M1_2M2)(O/OH)L1_3]L2$, where M1 and M2 are the metals in the trimer of the acs net, L1 is the dicarboxylate ligand for the formation of the pristine framework, and L2 is the tripyridyl pore-partitioning agent. The pore-partitioning agents not only partitioned the channel into smaller pores, but also deactivated all the open metal sites in the original acs framework. This process changed the adsorbents from ethylene-selective to ethane-selective. By experimental exploration of 9 compounds in this family, the authors demonstrated the exceptionally high ethane uptake of these ethane-selective adsorbents. In particular, CPM-233 (Mg_2V-bdc-tpt) took up 166 cm^3 g^{-1} (7.45 mmol g^{-1}) of ethane at 298 K and 1 bar, substantially higher than that for PCN-250 (117 cm^3 g^{-1}), the previous benchmark material for ethane uptake among ethane-selective adsorbents. In addition, the Q_{st} values for ethane in these materials were generally low, in the range of 21.9–30.4 kJ mol^{-1}, much lower than those with strong ethane-adsorption sites such as $Fe_2(O_2)$(dobdc). The relatively low adsorption heat may be advantageous with respect to energy consumption associated with adsorbent regeneration. The IAST

ethane/ethylene selectivities of these materials are between 1.4 and 1.75, comparable to those of most of the reported ethane-selective MOFs, but are significantly lower than those of the top-performing ones such as $Fe_2(O_2)$(dobdc) and $Cu(Qc)_2$. This study provided a valuable approach for achieving high adsorption capacity for ethane-selective MOFs. In a more recent study,[56] the same research group developed a series of MOFs built on 8-connected $M_3(OH)(OOCR)_5$(Py-R)$_3$ trimers (M = Zn, Co, Fe) through the so-called angle bending modulation strategy. Similar to the foregoing materials obtained *via* the PSP approach, these newly developed MOFs (CPM-80-82) exhibited favored adsorption of ethane over ethylene with high ethane uptake as well. For example, CPM-81-Co adsorbed 123 $cm^3\ g^{-1}$ of ethane at 298 K and 1 bar, with an ethane/ethylene IAST selectivity of 1.8.

The foregoing ethane-selective MOFs generally possess ethane/ethylene IAST selectivities of 1 to 4. In contrast, substantially higher ethane/ethylene selectivities have recently been achieved in a series of mesoporous MOFs (Fig. 9), the NIIC-20 family, developed by Fedin *et al.* They were built on Zn_{12}(-RCOO)$_{12}$(glycol)$_6$ rings, featuring 25 Å interconnected cages.[57] The materials were synthesized through solvothermal reactions of zinc nitrate, isophthalic acid, dabco, and the corresponding glycol in DMF. Taking NIIC-20-Bu as an example, it adsorbed 2.5 mmol g^{-1} of ethane at 298 K and 1 bar, notably higher than that of ethylene (1.4 mmol g^{-1}) under identical conditions, resulting in an ethane/ethylene IAST selectivity of 15.4 for an equimolar ethane/ethylene binary mixture. This selectivity is the new record for all ethane-selective adsorbents. Computational studies revealed that the preferential adsorption of ethane over ethylene in these materials originated from the stronger adsorption affinity of ethane in the nanocages, with the formation of strong C–H$\cdots$O hydrogen bonds.

Compared to the rapid development of ethane-selective adsorbents over the past few years, propane-selective adsorbents are much scarcer. A likely factor that may contribute to this is the smaller difference in molecular size and physical properties between propane and propylene, compared to that of ethane and ethylene. Xing *et al.* reported propane-selective propane/propylene separation by an anion-pillared microporous MOF, Ni(bpe)$_2$(WO_4) (WOFOUR-1-Ni).[45] Interestingly, the material adsorbed more propylene than propane at 298 K and 1 bar, but propane was favored at low pressure. The heat of adsorption for propane was also slightly higher than that of propylene. The calculated propane/propylene IAST selectivity was 1.6. Its propane-selective behavior was confirmed in the multicomponent column breakthrough measurements where propylene broke prior to propane. GCMC simulation and DFT calculations revealed that the preferential adsorption of propane over propylene originated from the stronger adsorption affinity of propane in the polycatenated molecular cages along with a certain degree of shape selectivity. More recently, Li *et al.* reported propane-selective adsorption by a modified UiO-type MOF, BUT-10.[46] Similar to that of the foregoing WOFOUR-1-Ni, BUT-10 also showed propane-favored adsorption at the relatively low pressure region, with higher adsorption affinity than that of propylene. It exhibited an IAST selectivity of 1.4, slightly lower than that of WOFOUR-1-Ni, but a much higher adsorption capacity for propane (105 $cm^3\ g^{-1}$) at 298 K and 1 bar.

Besides the foregoing experimental explorations for alkane-selective MOFs, computational studies exploiting the underlying adsorption mechanisms and design strategies have also been carried out by several research groups. Siperstein *et al.* applied GCMC simulations to investigate the influence of pore size and pore shape on ethane/ethylene selectivity in ethane-selective adsorbents.[87] They used a model by adding 4,4′-bipyridine pillars in slit pores to mimic MOF structures. With this simulation model, the authors successfully predicted the selectivity for many of the ethane-selective adsorbents. In particular, the authors concluded that ethane/ethylene adsorption selectivity based on van der Waals interactions cannot be higher than 2.8. However, higher selectivities toward ethane may be achieved if the MOF pores have strong electric field gradients that prevent the adsorption of ethylene or the pores are very small and fit better with ethane molecules. In another study, Jiang *et al.* performed a computational screening study on a large set (1747) of MOF structures and established quantitative relationships between adsorption performance (ethane/ethylene selectivity and capacity) and the structural descriptors (pore size, surface area, *etc.*).[88] The results indicated that the ethane/ethylene separation performance of a MOF is a complex interplay of the structural descriptors. Based on the computational findings, the authors proposed six design strategies for developing ethane-selective MOFs with high performance: regulating the topology, catenating the framework, adding an aromatic ring, pillar-layering the framework, substituting a metal node, and imposing flexibility.

Covalent organic frameworks (COFs) and hydrogen-bonded organic frameworks (HOFs) have also been explored for selective capture of ethane from ethane/ethylene mixtures. Li *et al.* reported the systematic regulation of pore channels in COFs for selective removal of ethane from ethylene.[89] Eight representative COFs with various pore sizes and pore environments, including COF-1, COF-6, COF-8, COF-10, MCOF-1, COF-102, COF-300, and COF-320, were selected for the evaluation of their adsorption and separation of ethane and ethylene. Several of them show a notable preference to ethane over ethylene, which was attributed to a large quantity of nonpolar benzene rings leading to strong C–H$\cdots\pi$ interactions with ethane. COF-1 was identified as the optimal adsorbent with an ethane/ethylene selectivity of 1.92 at 298 K and 1 bar, as a result of its richly distributed weakly polar surface and suitable pore dimensions. Chen *et al.* reported a series of microporous HOFs using hexacarboxylate ligands as building blocks.[90,91] These HOFs feature permanent porosity, good thermal stability, and high water resistance. Particularly, due to the nonpolar pore surfaces in these materials, they exhibit ethane-favored adsorption over ethylene with an ethane/ethylene selectivity of 2–3.

3. Kinetic separation

Compared to the foregoing thermodynamic separation, kinetic separation of alkane/alkene mixtures is relatively rare as it has stringent requirements on the pore size of MOFs (Table 2). Early

in 2009, Li *et al.* reported the kinetic separation of propane and propylene by ZIF-8 and its isoreticular $Zn(2\text{-cim})_2$.[92] While propane and propylene showed essentially identical adsorption capacity on these materials, they exhibited distinct adsorption kinetics. At 30 °C, the ratios of the diffusion rate coefficients, *D*(propane)/*D*(propylene), were 125 and 60 for ZIF-8 and $Zn(2\text{-cim})_2$, respectively. Obviously, the separation of propane and propylene by ZIF-8 and $Zn(2\text{-cim})_2$ was controlled by the critically sized pore openings. It was measured from the crystal structures that the pore apertures are 3.26 and 3.37 Å for ZIF-8 and $Zn(2\text{-cim})_2$, respectively.

In a subsequent study, Nguyen *et al.* carried out a systematic investigation on kinetic separation of propane and propylene in a series of isoreticular MOFs by tuning their pore apertures and crystallite aspect ratios.[93] These pillared paddlewheel MOFs built from 1,2,4,5-tetrakis(carboxyphenyl)benzene and *trans*-1,2-dipyridylethene linkers were synthesized solvothermally in DMF with the addition of aqueous hydrogen chloride. With a series of four isostructural MOFs, DTO, TO, DBTO, and BTO, with decreasing aperture size from 5.27 to 4.67 Å, they showed increasing propylene/propane kinetic selectivity from 1.4 to 12. Interestingly, the authors attempted to optimize the propylene/propane selectivity through tuning of the pore apertures (*via* –Br functionalization) and modulation of channel congestion (*via* the introduction of the TMS group). The results indicated that the former strategy exhibited noticeably more appreciable effects on the propylene/propane kinetic selectivity. In addition, an investigation of the influence of crystallite aspect ratios revealed that the orientation of the channel perpendicular to the largest faces of the crystals was necessary for achieving high kinetic selectivity. Li *et al.* explored the kinetic separation of propylene and propane on two ultramicroporous MOFs, $Zn(ox)_{0.5}(trz)$ and $Zn(ox)_{0.5}(atrz)$ (ox = oxalate, trz = 1,2,4-triazole, atrz = 3-amino-1,2,4-triazole).[94] These two compounds feature 1D zigzag channels with narrow necks of 2.9 and 2.6 Å for $Zn(ox)_{0.5}(trz)$ and $Zn(ox)_{0.5}(atrz)$, respectively. Both materials exhibited marked diffusional restrictions. The propylene/propane kinetic selectivity for $Zn(ox)_{0.5}(trz)$ reached 1565 at 323 K while for $Zn(ox)_{0.5}(atrz)$ the selectivity was 220. These values were substantially higher than those of the previously reported ZIF-8 and TO series. The high selectivities were attributed primarily to the appropriate pore apertures. Li *et al.* reported the kinetic separation of propylene and propane by ELM-12 ($Cu(bipy)_2(OTf)_2$, bipy = 4,4′-bipyridine, OTf = trifluoromethanesulfonate).[96] ELM-12 possesses zigzag 2D channels with a pore window of around 4.0 Å, and features high stability and facile scale-up preparation. The adsorption of propylene on ELM-12 showed no diffusional restrictions and reached equilibrium within 1–2 minutes. In contrast, severe diffusion limitations were observed for propane, resulting in propylene/propane kinetic selectivities of 204 and 971 at 298 and 308 K, respectively, comparable to those of $Zn(ox)_{0.5}(trz)$ and $Zn(ox)_{0.5}(atrz)$. The separation capability of ELM-12 was experimentally confirmed by column breakthrough measurements, which exhibited a clear separation for an equimolar propylene/propane binary mixture. Highly selective alkane/alkene separation may be achieved by tailoring the pore size or pore environment of MOFs, or by post-synthetic modification of their pore functionality. This was nicely demonstrated in the case of $Fe_2(O_2)$dobdc.

More recently, Zhang *et al.* reported the post-synthetic functionalization of MAF-23 to MAF-23-O and its kinetic separation of propane and propylene. MAF-23 is built on Zn(II) and btm^{2-} (H_2btm = bis(5-methyl-1*H*-1,2,4-triazol-3-yl)methane).[97] It showed no noticeable thermodynamic or kinetic separation toward propane and propylene (Fig. 10). Upon oxidation of MAF-23, btm^{2-} was converted to btk^{2-} (H_2btk = bis(5-methyl-1,2,4-triazol-3-yl)methanone), leading to the formation of MAF-23-O which retained the structure of MAF-23. The reaction was carried out by heating the pristine MAF-23 at 140 °C in

Table 2 Representative MOFs showing kinetic separation for alkane/alkene mixtures[a]

	MOF	BET surface area ($m^2\ g^{-1}$)	Aperture size (Å)	Uptake (mmol g^{-1})				
				Alkene	Alkane	Selec.	Temp. (K)	Ref.
C_3H_8/C_3H_6	ZIF-8	—	3.3	—	—	125	303	92
	$Zn(2\text{-cim})_2$	—	3.4	—	—	60	303	92
	DTO	669	5.3	—	—	1.4	298	93
	TO	512	5.4	—	—	2.5	298	93
	DBTO	457	5.1	—	—	11	298	93
	BTO	283	4.7	—	—	12	298	93
	$Zn(ox)_{0.5}(trz)$	546	2.9	2.3	—	860	303	94
	$Zn(ox)_{0.5}(atrz)$	521	2.6	1.7	—	175	303	94
	ftw-MOF-ABTC	—	4.4	2.3	2.5	—	298	95
	ELM-12	—	4.0	1.5	1.4	204	298	96
	MAF-23-O	—	3.6	1.4	1.2	71	298	97
	$Co_2(5\text{-aip})_2(bpy)$	—	—	2.0	0.5	21	298	98
	$ZnAtzPO_4$	420	3.8	1.1	0.3	31	298	99
C_2H_6/C_2H_4	GT-18	—	3	0.6	0.2	6.8	298	100
	Cu(OPTz)	—	—	2.3	0.4	6	300	101
	$ZnAtzPO_4$	—	4.9	1.9	1.0	12	298	102

[a] Notes: (1) gas uptakes were measured at the specified temperature and 1 bar. (2) Selectivities were calculated using the IAST model.

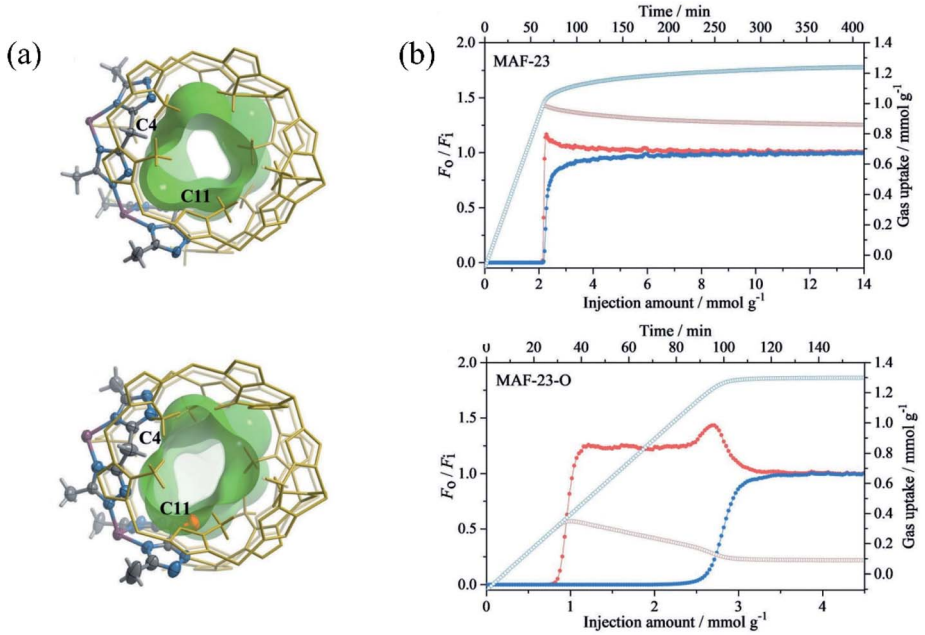

Fig. 10 (a) Crystal and pore structures of (top) MAF-23 and (bottom) MAF-23-O. The asymmetric units are drawn with thermal ellipsoids (50% probability). The two independent methylene/carbonyl groups are highlighted by atom labeling. (b) Breakthrough curves (solid) and adsorption kinetic curves (open) for (top) MAF-23 and (bottom) MAF-23-O using an equimolar C_3H_6/C_3H_8 (blue/red) mixture (1 cm^3 min^{-1}) at 298 K and 1 atm. Lines are drawn to guide the eye. F_i and F_o are the flow rates of each gas at the inlet and outlet, respectively. The negative gas uptakes shown in the initial regions are equal to the gas amount in the dead space of the breakthrough manifold. Reproduced with permission.[97] Copyright 2019, VCH.

oxygen for 1500 minutes. The conversion ratio of the oxidation reaction was 50%, meaning that both btm^{2-} and btk^{2-} were present in the newly formed compound. This subtle change in the organic linker dramatically affected the pore size and pore environment of the MOF, and thus noticeably improved its propane/propylene separation performance. The propylene/

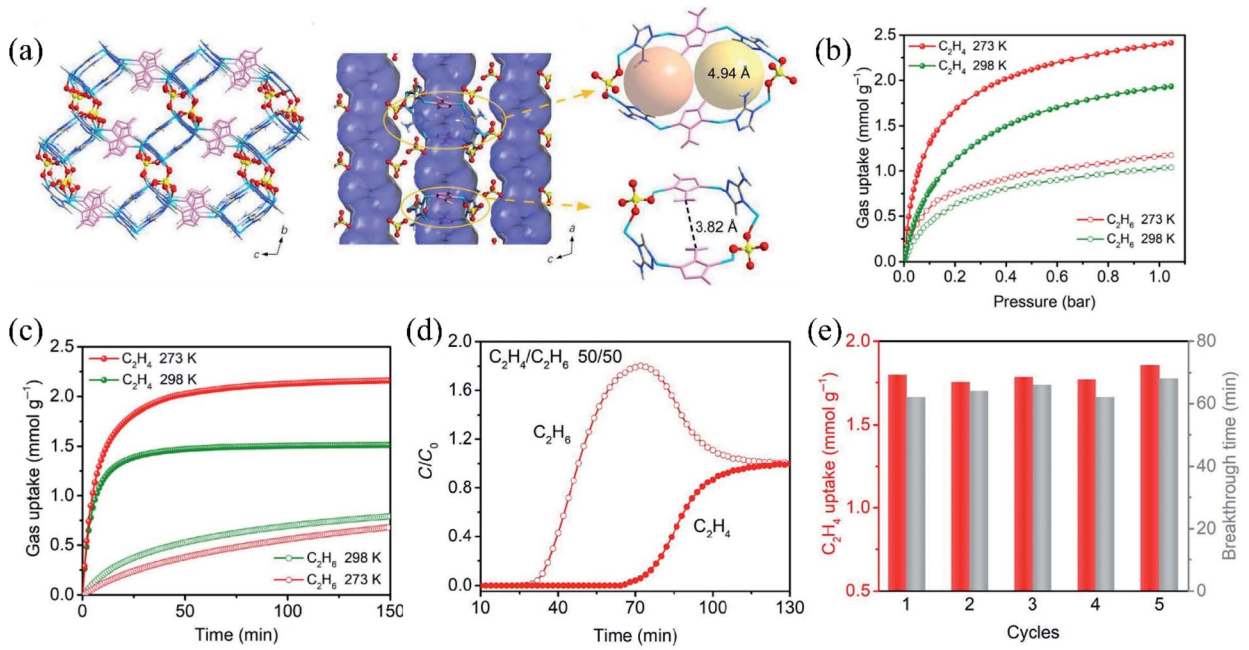

Fig. 11 (a) Schematic illustration of the structure of $ZnAtzPO_4$. (b) Single-component adsorption isotherms of C_2H_4 and C_2H_6 on $ZnAtzPO_4$ at 298 and 273 K. (c) Time-dependent gas uptake profiles of C_2H_4 and C_2H_6 at 0.4 bar and different temperatures. (d) Breakthrough curve of $ZnAtzPO_4$ for a C_2H_4/C_2H_6 gas mixture (50 : 50, v/v) at 273 K and 1 bar with a flow rate of 0.75 mL min^{-1}. (e) Recycling breakthrough tests for C_2H_4/C_2H_6 (50 : 50, v/v) separation with $ZnAtzPO_4$. Reproduced with permission.[102] Copyright 2020, AAAS.

propane kinetic selectivity was calculated to be 112.3 for MAF-23-O, two orders of magnitude higher than that of its parent structure. Interestingly, thermodynamic selectivity of propylene/propane was also enhanced as a result of the formation of the carbonyl bridges in the structure. The separation capability of MAF-23-O was confirmed by experimental column breakthrough measurements which yielded a propylene/propane selectivity of 15. This study demonstrated that the subtle structural change through post-synthetic modification may have a dramatic effect on kinetic and/or thermodynamic separation of alkane/alkene mixtures.

Kinetic separation of ethylene and ethane has been relatively rarely reported compared to that for propylene and propane. In a recent study, Lively *et al.* explored kinetically controlled separation of ethylene and ethane by a mixed-linker MOF, GT-18.[100] GT-18 was constructed on Zn(II) and two organic linkers, benzotriazole (BTA) and benzimidazole (BIM), with a molar ratio of 4 : 1. It features a similar structure to that of ZIF-7, with an aperture size of ~3 Å. While simulated adsorption isotherms for ethylene and ethane were almost identical, experimental isotherms under pseudo-equilibrium indicated that ethylene was noticeably favoured. Measurements of adsorption kinetics revealed that the diffusion of ethane was largely restricted compared to ethylene, leading to an ethylene/ethane kinetic selectivity of 6.8. This study demonstrates a simple strategy for fine-tuning MOF pore apertures for alkane/alkene kinetic separation by employing mixed linkers with suitable dimensions. Kitagawa *et al.* explored the adsorption of ethylene and ethane on a flexible porous coordination polymer, Cu(OPTz) (OPTz = phenothiazine-5,5-dioxide).[101] The compound features a flexible structure with flip-flop molecular motions within the framework that function as a gate for guest encapsulation and exclusion. Gas adsorption on Cu(OPTz) was highly temperature-dependent. Isobar measurements revealed that the adsorption capacity of ethylene increased as a function of increasing temperature and reached maximum capacity at 310 K, after which the adsorbed amount decreased with further increases in temperature. In contrast, the adsorption of ethane increased gradually as temperature increased and the adsorption capacity was noticeably lower than that for ethylene. Ethylene/ethane selectivity was calculated to be ~75 for Cu(OPTz). This study demonstrated making use of the temperature-dependent gating effect for the kinetic separation of ethane and ethylene.

Many of the foregoing separations result from a combined effect of thermodynamic separation and kinetic separation, but one dominates the other. However, in certain cases, both thermodynamic and kinetic mechanisms are the main contributors and show a markedly synergistic effect on alkane/alkene separation. Xia *et al.* reported the separation of propane and propylene by a pillar-layer MOF, $Zn_2(aip)_2(bpy)$ (aip = 5-aminoisophthalate, bpy = 4,4′-bipyridine).[42] The compound possesses 1D open channels and open metal sites upon removal of free and coordinated solvents. It adsorbed 1.99 mmol g^{-1} of propylene at 298 K and 1 bar, substantially higher than that for propane (0.48 mmol g^{-1}) under identical conditions. The calculated Q_{st} for propylene and propane was 42.4 and 33.7 kJ mol^{-1}, respectively, indicating higher interaction between the former and the framework. This resulted in a propylene/propane IAST selectivity of 19.8 for an equimolar binary mixture at 100 kPa. Experimental breakthrough measurements confirmed that the material was capable of separating propane and propylene with excellent recyclability. The authors concluded that the separation was based on an equilibrium mechanism; however, it is probably a combined effect of thermodynamic and kinetic mechanisms. This was confirmed in a subsequent study by the same group, where its analogue compound $Co_2(aip)_2(bpy)$ was studied for the adsorption and separation of propane and propylene.[98] $Co_2(aip)_2(bpy)$ exhibited similar separation performance for propane and propylene to its Zn-based analogue, with an IAST selectivity of 21. In this more recent work, the authors carried out additional computational simulations on the adsorption and separation mechanism, and observed the steric hindrance of propane and its low diffusion rate. This was further confirmed by kinetic adsorption experiments which yielded a propylene/propane kinetic selectivity of 29.7.

Xing *et al.* reported the equilibrium-kinetic synergetic effect for separation of ethylene and ethane by a microporous MOF,

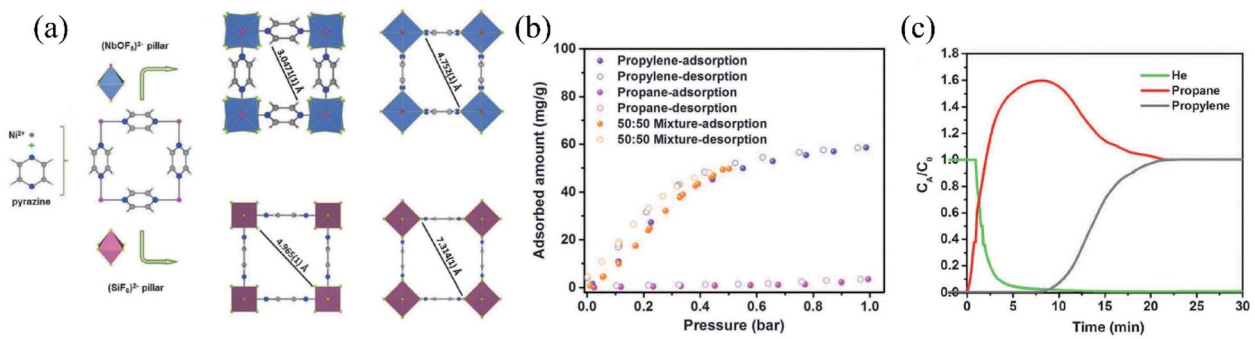

Fig. 12 (a) Structural description of NbOFFIVE-1-Ni (KAUST-7) highlighting the building block arrangement and its comparison with the parent SIFSIX-3-Ni. (b) The pure C_3H_8 (pink), pure C_3H_6 (purple), and equimolar mixture of C_3H_6/C_3H_8 50/50 (orange) isotherms of NbOFFIVE-1-Ni collected at 298 K, demonstrating the full propylene-from-propane sieving ability of this adsorbent at 1 bar. (c) C_3H_6/C_3H_8 50/50 mixed-gas experiment using a packed column bed at 298 K and a 1 bar total pressure and 4 cm^3 min^{-1} total flow, confirming the infinite C_3H_6/C_3H_8 separation factor. Reproduced with permission.[13] Copyright 2016, AAAS.

$ZnAtzPO_4$ (Atz = 3-amino-1,2,4-triazole) (Fig. 11).[102] $ZnAtzPO_4$ was prepared solvothermally with $3Zn(OH)_2 \cdot 2ZnCO_3$, Atz, and phosphoric acid in a mixed solvent of water and ethanol. The compound is built on 2D ZnAtz cationic layers pillared by PO_4^{3-} anions forming a 3D porous framework. The material possesses 1D channels with narrow necks (3.82 Å) and wider chambers (4.94 Å) with the channels decorated by electronegative amino groups from Atz ligands and oxygen atoms from PO_4^{3-} anions. Adsorption isotherms at 298 K revealed that its ethylene uptake was 1.92 mmol g^{-1} at 1 bar, notably higher than that for ethane (1.01 mmol g^{-1}) under identical conditions. Kinetic studies indicated that the adsorption of ethylene reached equilibrium within about 40 minutes at 298 K, substantially faster than that for ethane which did not reach equilibrium after 150 minutes. The difference in adsorption rates yielded an ethylene/ethane kinetic selectivity of 36.6 at 298 K. The authors further calculated the equilibrium-kinetic combined selectivity based on their diffusivities and Henry's constants. $ZnAtzPO_4$ exhibited a combined selectivity of 12.4 at 298 K, higher than those of other kinetically selective adsorbents such as ITQ-55 and Si-CHA under identical conditions. DFT calculations revealed that there were two primary adsorption sites for ethylene molecules where they interact with the pores through multiple hydrogen bonds. In contrast, the adsorption of ethane in the pore induced notable steric hindrance. It is noteworthy that the Q_{st} for ethylene on $ZnAtzPO_4$ was 17.3, substantially lower than that on other adsorbents with or without OMSs. This may be beneficial for material regeneration and was confirmed by column breakthrough measurements. The material showed excellent recyclability under ambient regeneration through purging with inert gas. In a more recent report,[99] the same research group demonstrated that $ZnAtzPO_4$ showed similar equilibrium-kinetic separation for propane and propylene. In contrast to ethylene which reached adsorption equilibrium within 40 minutes, the adsorption of propylene did not reach equilibrium after 180 minutes. And the adsorption of propane was even slower. This resulted in a propylene/propane kinetic selectivity of 11 and an equilibrium-kinetic combined selectivity of 8.5 at 298 K. Similarly, the material featured relatively low heats of adsorption for propylene (27.5 kJ mol^{-1}) leading to mild regeneration conditions under column separation.

4. Selective size exclusion

Separation based on selective size exclusion occurs as a special scenario of kinetic separation, where the pore size of the adsorbent is optimal leading to one or more adsorbates being adsorbed while the others are completely excluded. It is considered the ideal separation as it offers the highest possible adsorption selectivity. However, separation through selective size exclusion has a stringent requirement on pore size, especially for the alkane/alkene separation where the differences in molecular dimensions are minor. Compared to traditional adsorbent materials, MOFs hold particular promise for selective size exclusion due to their diverse structures and highly tunable pore size. Over the past few years, several MOFs showing selective size-exclusion for alkane/alkene separation have been developed (Table 3).

KAUST-7 (also denoted as NbOFFIVE-1-Ni) developed by Eddaoudi *et al.* is the first MOF showing complete sieving of alkane/alkene mixtures (Fig. 12).[13] It adsorbs propylene but fully excludes propane. It is worth mentioning that the material was rationally designed through a reticular chemistry approach. The structure of KAUST-7 is built on Ni(II)–pyrazine square-grid layers pillared by $NbOF_5^{2-}$ struts. The material was prepared hydrothermally with $Ni(NO_3)_2 \cdot 6H_2O$ and Nb_2O_5 with the addition of HF. It is a derivative compound of the previously developed SIFSIX-3-Ni with SiF_6^{2-} substituted by $NbOF_5^{2-}$ aiming at downsizing the pore aperture. The resultant KAUST-7 obtained through topology-directed structure tuning retains the primitive cubic topology with a reduced pore aperture of 3.0 to 4.8 Å, depending on the rotation of the $NbOF_5^{2-}$ pillars. At 298 K and 1 bar, KASUT-7 adsorbs 60 mg g^{-1} of propylene, but shows essentially no adsorption of propane under identical conditions. This should be attributed to its optimal pore dimensions. The selective molecular exclusion behavior was confirmed by simultaneous calorimetric and gravimetric measurements which show a heat of adsorption of 57.4 kJ mol^{-1} for propylene while no detectable heat change was observed for propane. Multicomponent column breakthrough measurements indicated that KASUT-7 is capable of fully separating propane and propylene. Propane broke out at the outlet immediately without any retention, which confirmed that it was fully excluded by the adsorbent. In contrast, propylene

Table 3 Representative MOFs showing selective molecular exclusion for alkane/alkene mixtures[a]

	MOF	BET surface area (m^2 g^{-1})	Aperture size (Å)	Uptake (mmol g^{-1})		Temp. (K)	Ref.
				alkene	alkane		
C_3H_8/C_3H_6	KAUST-7	280	4.7	1.4	<0.1	298	13
	Y-abtc	427	4.7	2.0	<0.1	298	103
	Co-gallate	486	5.2	1.8	<0.1	298	104
C_2H_6/C_2H_4	Co-gallate	475	5.0	5.2	0.3	298	105
	Mg-gallate	559	4.8	4.3	0.3	298	105
	Ni-gallate	424	4.8	3.1	0.3	298	105
	UTSA-280	331	3.8	2.5	<0.1	298	21

[a] Notes: (1) gas uptakes were measured at the specified temperature and 1 bar. (2) Selectivities were calculated using the IAST model.

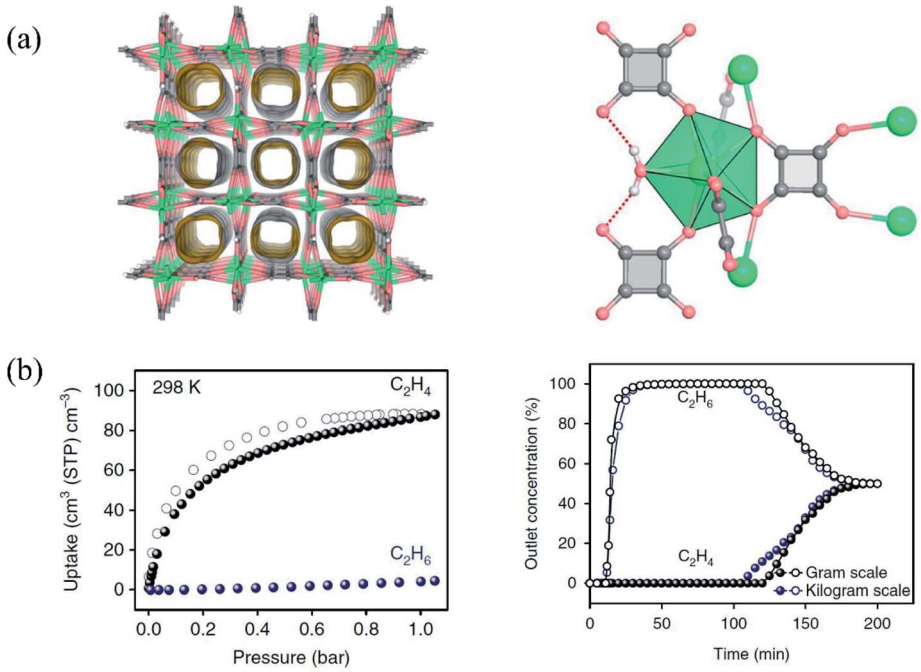

Fig. 13 (a) The crystal structure of guest-free UTSA-280 determined from single-crystal X-ray diffraction, showing one-dimensional channels viewed along the [001] direction. Green, light coral and grey nodes represent Ca, O and C atoms, respectively, and the local coordination environments of the squarate linker and calcium atoms. (b) (Left) Single-component sorption isotherms of ethylene (black) and ethane (blue) at 298 K and (right) breakthrough curves for UTSA-280 from different scales for an equimolar binary mixture of C_2H_4/C_2H_6 at 298 K and 1 bar. The breakthrough experiments were carried out in a packed column with 3.2 g sample at a flow rate of 2 mL min^{-1}. The points are experimental data, and the lines are drawn to guide the eye. Reproduced with permission.[21] Copyright 2018, Springer Nature.

was retained in the column for 8 minutes, equivalent to a dynamic adsorption capacity of 0.6 mmol g^{-1}. To evaluate the separation capability of KAUST-7 relating to industrial conditions, the authors applied a concentration swing recycling mode (CSRM) over multiple adsorption–desorption cycles, resulting in a propylene recovery of 2 mol kg^{-1} h^{-1}. KAUST-7 outperformed zeolite 4A and 5A under identical conditions. In this work the authors demonstrated the power of reticular chemistry in fine-tuning the pore dimensions of MOFs for challenging size-sieving separations.

In a subsequent study,[103] Li *et al.* reported the separation of propane and propylene through selective size exclusion by Y-abtc ($Y_6(OH)_8(abtc)_3(H_2O)_6(DMA)_2$) ($abtc^{4-}$ = 3,3′,5,5′-azobenzene-tetracarboxylates; DMA = dimethylammonium). The compound was tailor-made through topology-directed pore size tuning of the ftw-type structure based on hexanuclear Zr(IV) or Y(III) clusters. In this work the authors demonstrated the important role of charge balancing dimethylammonium (DMA) cations in Y-MOFs as a regulatory factor to fine tune and control pore dimensions. With a tetratopic ligand, Y-ftw-MOF and Zr-ftw-MOF feature similar connectivity with the former resulting in an anionic framework and the latter a cationic one. Thus the pore size of the Y-ftw-MOF is smaller than that of the Zr analogue due to the existence of the charge balancing cation. For the same ligand $abtc^{4-}$, Zr-abtc adsorbed both propane and propylene, with similar adsorption capacities and kinetics, showing no separation. In contrast, Y-abtc adsorbed propylene only and fully excluded propane, exhibiting selective molecular exclusion behavior. This should be attributed to its optimal pore size of 4.72 Å. Investigation of adsorption kinetics revealed that it is a case of selective size sieving rather than kinetic separation. Multicomponent column breakthrough measurements confirmed that Y-abtc is capable of full separation of propane and propylene and produces highly pure propylene (99.5+%) that meets the requirements for polymer production. Interestingly, the authors revealed the pore size regulation mechanism by the DMA cations. With relatively low activation temperature, the DMA cations remained intact and the pore size of the MOF is relatively small. However, with increased activation temperature, its pore size increased as DMA cations were converted to protons. This was experimentally confirmed by NMR and gas adsorption studies. The material design strategy in this work may be useful in future development of ideal adsorbents for efficient alkane/alkene separation.

Bao *et al.* reported the separation of ethane and ethylene through selective molecular sieving by gallate-based MOFs, Ni/Mg/Co-gallate.[105] These MOFs feature 3D interconnected zigzag channels with pore dimensions of 3.47 × 4.85, 3.56 × 4.84, and 3.69 × 4.95 $Å^2$ for Ni, Mg, and Co-gallate, respectively, which are slightly larger than the minimum cross-section size of ethylene. As expected, these compounds adsorbed a substantial amount of ethylene but negligible ethane under identical conditions. Taking Co-gallate as an example, its uptake of ethylene is 3.37 mmol g^{-1} at 298 K and 1 bar, notably higher than that of ethane (0.31 mmol g^{-1}). Multicomponent column breakthrough measurements confirmed that ethane and ethylene can

be fully separated by these materials. Interestingly, more recently, Chen *et al.* reported the full separation of propane and propylene, using the same material, Co-gallate.[104] It adsorbed 66.6 $cm^3\ cm^{-3}$ of propylene at 298 K and 1 bar, while its uptake for propane was negligible (<6 $cm^3\ cm^{-3}$), suggesting its selective molecular sieving behavior. With respect to the volumetric adsorption capacity of propylene, Co-gallate outperforms KAUST-7 and Y-abtc, the other two MOFs showing selective molecular sieving for propane and propylene, although its gravimetric uptake is lower. Its separation capability was confirmed by column breakthrough measurements which showed complete separation of the two gases. With an equimolar binary mixture as a feed, propylene with a purity of 97.7% was produced through a single PSA process. These two studies suggest that with optimal pore shape and pore size, one adsorbent may be capable of separating both propane/propylene and ethane/ethylene through selective size sieving.

Another important study in adsorptive separation of ethylene and ethane by MOFs was reported by Chen *et al.* in 2018,[21] where selective molecular exclusion was achieved by $Ca(C_4O_4)(H_2O)$ (or UTSA-280, $H_2C_4O_4$ = squaric acid, Fig. 13). The compound was originally reported in 1987,[106] featuring a 3D framework with 1D channels. The material features facile synthesis, and can be prepared at a large scale at room temperature by mixing a saturated aqueous solution of sodium squarate with an aqueous solution of calcium nitrate. The cross-sectional area of the channels is 14.4 $Å^2$, falling between the minimum cross-sectional areas of ethylene (13.7 $Å^2$) and ethane (15.5 $Å^2$), indicating its potential for the separation of the two gases. Indeed, experimental gas adsorption measurements confirmed that UTSA-280 was capable of splitting ethane and ethylene. It adsorbed 2.5 mmol g^{-1} of ethylene at 298 K and 1 bar while ethane was essentially excluded by the material (uptake < 0.1 mmol g^{-1}) under identical conditions. The matching between the size/shape of ethylene and the channel dimensions led to its relatively high adsorption capacity. This was confirmed by gas-loaded single-crystal X-ray diffraction and computational modeling. The crystal structure of ethylene-loaded UTSA-280 revealed that ethylene molecules adopted optimal orientation, with its minimum cross-section along the diagonal of the pore aperture to minimize any possible steric hindrance and electrostatic repulsion from the framework. In contrast, significant steric hindrance will be unavoidable when ethane molecules are put inside the channels with random orientations, in good agreement with the noticeably higher potential energy variations for ethane along the channels from DFT calculations. The ethane/ethylene separation ability of UTSA-280 was confirmed by column breakthrough measurements with binary ethane/ethylene and octonary $H_2/CH_4/C_2H_2/C_2H_4/C_2H_6/C_3H_6/C_3H_8/C_4H_8$ mixtures. The results indicated that the adsorbent was capable of enriching ethylene from the complicated mixtures, indicating its excellent capability for the purification of ethylene.

Very recently, Zhang and coworkers reported full separation of ethane and ethylene by a HOF material through a gating mechanism.[107] The material, HOF-FJU-1, was constructed from a tetracyano-bicarbazole building block, which possessed permanent porosity and a flexible framework. As a result of the structural flexibility, the adsorption of ethane and ethylene on HOF-FJU-1 exhibited a gating behavior and was highly temperature-dependent. At 318 and 333 K, it adsorbed ethylene only and fully excluded ethane, showing a molecular sieving behavior. Column breakthrough measurements confirmed the capability of HOF-FJU-1 for the capture of ethylene from a mixture of ethylene, ethane, propylene, propane, methane, and hydrogen.

5. Conclusion and outlook

In this review, we provide an overview of the major advancements in C_2–C_3 alkane/alkene separation by metal–organic frameworks. We present the research progress based on three separation mechanisms: thermodynamic separation (including alkane-selective and alkene-selective), kinetic separation, and selective size exclusion-based separation. Representative examples in each category are discussed and material design strategies and structure–property relationships are emphasized. It is exciting to witness the tremendous progress in the development of tailored MOFs for highly efficient separation of alkanes and alkenes over the past few years, particularly that of alkane-selective MOFs with relatively high adsorption selectivity. In addition, several MOFs that are capable of separating alkane and alkene mixtures *via* selective molecular exclusion have been achieved through rational design. These achievements demonstrate that MOFs are indeed promising adsorbent materials for the separation of alkanes/alkenes. Some of them have already outperformed traditional adsorbents for certain separation processes.

The potential of MOFs for alkane/alkene separation has been well illustrated in this review article. However, some concerns and challenges need to be addressed in the future development of MOFs for their implementation in industries: (1) material stability. MOFs have suffered from relatively poor stability compared to conventional inorganic adsorbents since they first emerged. This issue has been partially addressed over the past decade by various approaches, such as the incorporation of early transition metals as inorganic building units. Some of the MOFs presented in this article are sensitive to moisture or air, which limits their application even though they may have excellent separation performance. Material stability and long-term durability would be the primary aspects to consider for developing MOFs for industrial applications. In addition to thermal and moisture stability, their resistance to other gaseous impurities that are present in the stream should be assessed. For example, Eddaoudi *et al.* evaluated the stability of KAUST-7 under H_2S exposure when exploring its potential for propane/propylene separation.[13] Similar experiments are recommended for all adsorbents that are aimed for alkane/alkene separation applications. (2) Trade-off between adsorption capacity and selectivity. It is noteworthy from the overview in this article that some MOFs have either high adsorption capacity or adsorption selectivity for alkane/alkene separation, but seldomly have both. For example, the adsorption capacities for those showing selective molecular exclusion are typically low. A way to

potentially resolve this issue is to rely on the rational design of materials. Reticular chemistry can guide researchers to precisely control the resulting structures with an ideal topology/pore structure or to introduce an optimal adsorption site. (3) Evaluation conditions. Practical conditions of alkane/alkene separation may differ, depending on the source of feed mixtures. For example, propane/propylene mixtures from steam cracking of naphtha are usually equimolar, while the mixture from fluid catalytic cracking has 80+% propylene. Thus, for a specific separation process it is important to determine whether alkane-selective or alkene-selective adsorbents are preferred and the optimal conditions for the adsorbent. Moreover, the adsorption and separation capability of MOFs should be evaluated under industrially relevant conditions including other minor components likely to be present in an industrial scenario, rather than a mixture of pure olefin and paraffin. (4) Cost. Compared with conventional adsorbent materials, the synthesis of MOFs is generally more expensive, especially when large, complex organic linkers are involved. Future endeavours in preparing cost effective yet highly robust MOFs with desirable porosity using inexpensive ligands are much needed for real-world applications.

Effective separation of alkanes and alkenes is of paramount importance in the petrochemical industry for various uses, for example, to produce high purity ethylene and propylene. These processes currently rely on cryogenic distillation, suggesting that ideal adsorbents for adsorptive separation are yet to be developed. To the best of our knowledge, neither zeolites nor MOFs have been used for industrial separation of alkane and alkene mixtures so far. However, they are the current research focus in the scientific community and represent the two most promising types of adsorbent that may become suitable candidates for industrial implementation. Zeolites are well explored, highly stable, and relatively inexpensive. On the other hand, MOFs are a relatively new adsorbent class with numerous advantages. The exploration of MOFs for adsorptive alkane/alkene separation is undergoing a very rapid growth. Although challenges remain for the industrial implementation of MOFs, including stability, cost, *etc.*, their exceptionally tunable structure and pore geometry/size, and diverse gas–framework interactions make them highly valuable for both fundamental research and industrial applications. While some of the challenges may be difficult to overcome, with the tireless efforts of many researchers working in the field, we are confident that great advancements will continue to be made and the future is bright for the development of MOF-based adsorbents suitable for separation of alkanes and alkenes.

Conflicts of interest

There are no conflicts to declare.

Acknowledgements

We thank the National Natural Science Foundation of China (No. 21901166), Natural Science Foundation of Guangdong Province (No. 2019A1515010692), Shenzhen Science and Technology Program (No. JCYJ20190809145615620, RCYX20200714114539243) and the U. S. Department of Energy, Office of Science, Office of Basic Energy Sciences (DE-SC0019902) for the financial support.

Notes and references

1 R. A. Myers, *Handbook of Petroleum Refining Processes*, McGraw-Hill, New York, 2004.
2 R. Lively, *Nature*, 2016, **532**, 435–437.
3 P. J. Bereciartua, Á. Cantín, A. Corma, J. L. Jordá, M. Palomino, F. Rey, S. Valencia, E. W. Corcoran, P. Kortunov, P. I. Ravikovitch, A. Burton, C. Yoon, Y. Wang, C. Paur, J. Guzman, A. R. Bishop and G. L. Casty, *Science*, 2017, **358**, 1068.
4 Y. Liu, Y. Wu, W. Liang, J. Peng, Z. Li, H. Wang, M. J. Janik and J. Xiao, *Chem. Eng. Sci.*, 2020, **220**, 115636.
5 D. Saha, B. Toof, R. Krishna, G. Orkoulas, P. Gismondi, R. Thorpe and M. L. Comroe, *Microporous Mesoporous Mater.*, 2020, **299**, 110099.
6 P. Zhang, X. Wen, L. Wang, Y. Zhong, Y. Su, Y. Zhang, J. Wang, J. Yang, Z. Zeng and S. Deng, *Chem. Eng. J.*, 2020, **381**, 122731.
7 C. Yu, M. G. Cowan, R. D. Noble and W. Zhang, *Chem. Commun.*, 2014, **50**, 5745–5747.
8 L. Huang and D. Cao, *J. Mater. Chem. A*, 2013, **1**, 9433–9439.
9 B. Li, Y. Zhang, R. Krishna, K. Yao, Y. Han, Z. Wu, D. Ma, Z. Shi, T. Pham, B. Space, J. Liu, P. K. Thallapally, J. Liu, M. Chrzanowski and S. Ma, *J. Am. Chem. Soc.*, 2014, **136**, 8654–8660.
10 M. C. Campo, A. M. Ribeiro, A. Ferreira, J. C. Santos, C. Lutz, J. M. Loureiro and A. E. Rodrigues, *Sep. Purif. Technol.*, 2013, **103**, 60–70.
11 J. Gi Min, K. Christian Kemp, K. S. Kencana, R. R. Mukti and S. Bong Hong, *Chem. Eng. J.*, 2021, **413**, 127422.
12 M. Khalighi, I. A. Karimi and S. Farooq, *Ind. Eng. Chem. Res.*, 2014, **53**, 16973–16983.
13 A. Cadiau, K. Adil, P. M. Bhatt, Y. Belmabkhout and M. Eddaoudi, *Science*, 2016, **353**, 137.
14 H. Wang, Y. Liu and J. Li, *Adv. Mater.*, 2020, **32**, 2002603.
15 W.-G. Cui, T.-L. Hu and X.-H. Bu, *Adv. Mater.*, 2020, **32**, 1806445.
16 J. Pei, K. Shao, L. Zhang, H.-M. Wen, B. Li and G. Qian, *Top. Curr. Chem.*, 2019, **377**, 33.
17 K. Adil, Y. Belmabkhout, R. S. Pillai, A. Cadiau, P. M. Bhatt, A. H. Assen, G. Maurin and M. Eddaoudi, *Chem. Soc. Rev.*, 2017, **46**, 3402–3430.
18 Z. R. Herm, E. D. Bloch and J. R. Long, *Chem. Mater.*, 2014, **26**, 323–338.
19 Z. Bao, G. Chang, H. Xing, R. Krishna, Q. Ren and B. Chen, *Energy Environ. Sci.*, 2016, **9**, 3612–3641.
20 L. Li, R.-B. Lin, R. Krishna, H. Li, S. Xiang, H. Wu, J. Li, W. Zhou and B. Chen, *Science*, 2018, **362**, 443.
21 R.-B. Lin, L. Li, H.-L. Zhou, H. Wu, C. He, S. Li, R. Krishna, J. Li, W. Zhou and B. Chen, *Nat. Mater.*, 2018, **17**, 1128–1133.

22 T. M. Nicholson and S. K. Bhatia, *J. Phys. Chem. B*, 2006, **110**, 24834–24836.
23 T. M. Nicholson and S. K. Bhatia, *Adsorpt. Sci. Technol.*, 2007, **25**, 607–619.
24 S. Wang, Q. Yang and C. Zhong, *Sep. Purif. Technol.*, 2008, **60**, 30–35.
25 (*a*) N. Lamia, *et al.*, *Chem. Eng. Sci.*, 2009, **64**, 3246–3259; (*b*) J. W. Yoon, *et al.*, *Bull. Korean Chem. Soc.*, 2010, **31**(1), DOI: 10.5012/bkcs.2010.31.01.220.
26 Y. Sun, Z. Ke, Y. Tang, S. Wang, Y. Wu, Q. Xia and Z. Li, *Ind. Eng. Chem. Res.*, 2020, **59**, 6202–6209.
27 J. W. Yoon, Y.-K. Seo, Y. K. Hwang, J.-S. Chang, H. Leclerc, S. Wuttke, P. Bazin, A. Vimont, M. Daturi, E. Bloch, P. L. Llewellyn, C. Serre, P. Horcajada, J.-M. Grenèche, A. E. Rodrigues and G. Férey, *Angew. Chem., Int. Ed.*, 2010, **49**, 5949–5952.
28 Y.-S. Bae, C. Y. Lee, K. C. Kim, O. K. Farha, P. Nickias, J. T. Hupp, S. T. Nguyen and R. Q. Snurr, *Angew. Chem., Int. Ed.*, 2012, **51**, 1857–1860.
29 Z. Bao, S. Alnemrat, L. Yu, I. Vasiliev, Q. Ren, X. Lu and S. Deng, *Langmuir*, 2011, **27**, 13554–13562.
30 E. D. Bloch, W. L. Queen, R. Krishna, J. M. Zadrozny, C. M. Brown and J. R. Long, *Science*, 2012, **335**, 1606.
31 S. J. Geier, J. A. Mason, E. D. Bloch, W. L. Queen, M. R. Hudson, C. M. Brown and J. R. Long, *Chem. Sci.*, 2013, **4**, 2054–2061.
32 J. E. Bachman, M. T. Kapelewski, D. A. Reed, M. I. Gonzalez and J. R. Long, *J. Am. Chem. Soc.*, 2017, **139**, 15363–15370.
33 G. Chang, M. Huang, Y. Su, H. Xing, B. Su, Z. Zhang, Q. Yang, Y. Yang, Q. Ren, Z. Bao and B. Chen, *Chem. Commun.*, 2015, **51**, 2859–2862.
34 L. Zhang, L. Li, E. Hu, L. Yang, K. Shao, L. Yao, K. Jiang, Y. Cui, Y. Yang, B. Li, B. Chen and G. Qian, *Adv. Sci.*, 2020, **7**, 1901918.
35 X. Wang, P. Zhang, Z. Zhang, L. Yang, Q. Ding, X. Cui, J. Wang and H. Xing, *Ind. Eng. Chem. Res.*, 2020, **59**, 3531–3537.
36 S. Yang, A. J. Ramirez-Cuesta, R. Newby, V. Garcia-Sakai, P. Manuel, S. K. Callear, S. I. Campbell, C. C. Tang and M. Schröder, *Nat. Chem.*, 2015, **7**, 121–129.
37 X. Wang, R. Krishna, L. Li, B. Wang, T. He, Y.-Z. Zhang, J.-R. Li and J. Li, *Chem. Eng. J.*, 2018, **346**, 489–496.
38 K.-J. Chen, D. G. Madden, S. Mukherjee, T. Pham, K. A. Forrest, A. Kumar, B. Space, J. Kong, Q.-Y. Zhang and M. J. Zaworotko, *Science*, 2019, **366**, 241.
39 E. D. Bloch, *et al.*, *Science*, 2012, **335**(6076), 1606–1610.
40 M. Hartmann, U. Böhme, M. Hovestadt and C. Paula, *Langmuir*, 2015, **31**, 12382–12389.
41 A.-R. Kim, T.-U. Yoon, E.-J. Kim, J. W. Yoon, S.-Y. Kim, J. W. Yoon, Y. K. Hwang, J.-S. Chang and Y.-S. Bae, *Chem. Eng. J.*, 2018, **331**, 777–784.
42 Y. Chen, H. Wu, D. Lv, N. Yuan, Q. Xia and Z. Li, *Sep. Purif. Technol.*, 2018, **204**, 75–80.
43 S.-Y. Kim, T.-U. Yoon, J. H. Kang, A.-R. Kim, T.-H. Kim, S.-I. Kim, W. Park, K. C. Kim and Y.-S. Bae, *ACS Appl. Mater. Interfaces*, 2018, **10**, 27521–27530.
44 Z. Chang, R.-B. Lin, Y. Ye, C. Duan and B. Chen, *J. Mater. Chem. A*, 2019, **7**, 25567–25572.
45 L. Yang, X. Cui, Q. Ding, Q. Wang, A. Jin, L. Ge and H. Xing, *ACS Appl. Mater. Interfaces*, 2020, **12**, 2525–2530.
46 C. He, Y. Wang, Y. Chen, X. Wang, J. Yang, L. Li and J. Li, *Chem. Eng. J.*, 2021, **403**, 126428.
47 S. Wang, Y. Zhang, Y. Tang, Y. Wen, Z. Lv, S. Liu, X. Li and X. Zhou, *Chem. Eng. Sci.*, 2020, **219**, 115604.
48 U. Böhme, B. Barth, C. Paula, A. Kuhnt, W. Schwieger, A. Mundstock, J. Caro and M. Hartmann, *Langmuir*, 2013, **29**, 8592–8600.
49 H. Bigdelou, M. R. Khosravi-Nikou and A. Shariati, *Chem. Eng. Res. Des.*, 2020, **159**, 315–327.
50 H. Xiang, A. Ameen, J. Shang, Y. Jiao, P. Gorgojo, F. R. Siperstein and X. Fan, *Microporous Mesoporous Mater.*, 2020, **293**, 109784.
51 Y. Yin, Z. Zhang, C. Xu, H. Wu, L. Shi, S. Wang, X. Xu, A. Yuan, S. Wang and H. Sun, *ACS Sustainable Chem. Eng.*, 2020, **8**, 823–830.
52 Y. Wang, S. Yuan, Z. Hu, T. Kundu, J. Zhang, S. B. Peh, Y. Cheng, J. Dong, D. Yuan, H.-C. Zhou and D. Zhao, *ACS Sustainable Chem. Eng.*, 2019, **7**, 7118–7126.
53 L. Li, L. Guo, S. Pu, J. Wang, Q. Yang, Z. Zhang, Y. Yang, Q. Ren, S. Alnemrat and Z. Bao, *Chem. Eng. J.*, 2019, **358**, 446–455.
54 Y. Wang, Z. Hu, Y. Cheng and D. Zhao, *Ind. Eng. Chem. Res.*, 2017, **56**, 4508–4516.
55 K. H. Cho, J. W. Yoon, J. H. Lee, J. C. Kim, K. Kim, U. H. Lee, S. K. Kwak and J.-S. Chang, *Microporous Mesoporous Mater.*, 2020, **307**, 110473.
56 X.-W. Lei, H. Yang, Y. Wang, Y. Wang, X. Chen, Y. Xiao, X. Bu and P. Feng, *Small*, 2020, 2003167.
57 A. A. Lysova, D. G. Samsonenko, K. A. Kovalenko, A. S. Nizovtsev, D. N. Dybtsev and V. P. Fedin, *Angew. Chem., Int. Ed.*, 2020, **59**, 20561–20567.
58 O. T. Qazvini, L. K. Macreadie and S. G. Telfer, *Chem. Mater.*, 2020, **32**, 6744–6752.
59 O. T. Qazvini, R. Babarao, Z.-L. Shi, Y.-B. Zhang and S. G. Telfer, *J. Am. Chem. Soc.*, 2019, **141**, 5014–5020.
60 Y. Lin, Y. Li, H. Wang, D. Luo, F. Lin and J. Li, *New J. Chem.*, 2020, **44**, 11933–11936.
61 H. Xiang, Y. Shao, A. Ameen, H. Chen, W. Yang, P. Gorgojo, F. R. Siperstein, X. Fan and Q. Pan, *Sep. Purif. Technol.*, 2020, **242**, 116819.
62 A. Dinh, H. Yang, F. Peng, T. C. Nguyen, A. Hong, P. Feng and X. Bu, *Cryst. Growth Des.*, 2020, **20**, 3523–3530.
63 C. He, Y. Wang, Y. Chen, X. Wang, J. Yang, L. Li and J. Li, *Ind. Eng. Chem. Res.*, 2020, **59**, 6123–6129.
64 L. Yang, Y. Wang, Y. Chen, J. Yang, X. Wang, L. Li and J. Li, *Chem. Eng. J.*, 2020, **387**, 124137.
65 Y. Tang, S. Wang, X. Zhou, Y. Wu, S. Xian and Z. Li, *Chem. Eng. Sci.*, 2020, **213**, 115355.
66 R.-B. Lin, H. Wu, L. Li, X.-L. Tang, Z. Li, J. Gao, H. Cui, W. Zhou and B. Chen, *J. Am. Chem. Soc.*, 2018, **140**, 12940–12946.
67 F.-Z. Sun, S.-Q. Yang, R. Krishna, Y.-H. Zhang, Y.-P. Xia and T.-L. Hu, *ACS Appl. Mater. Interfaces*, 2020, **12**, 6105–6111.

68 J. Pei, J.-X. Wang, K. Shao, Y. Yang, Y. Cui, H. Wu, W. Zhou, B. Li and G. Qian, *J. Mater. Chem. A*, 2020, **8**, 3613–3620.
69 L. Yang, W. Zhou, H. Li, A. Alsalme, L. Jia, J. Yang, J. Li, L. Li and B. Chen, *Chin. J. Chem. Eng.*, 2020, **28**, 593–597.
70 H. Yang, Y. Wang, R. Krishna, X. Jia, Y. Wang, A. N. Hong, C. Dang, H. E. Castillo, X. Bu and P. Feng, *J. Am. Chem. Soc.*, 2020, **142**, 2222–2227.
71 H. Xiang, A. Ameen, P. Gorgojo, F. R. Siperstein, S. M. Holmes and X. Fan, *Microporous Mesoporous Mater.*, 2020, **292**, 109724.
72 W. Liang, F. Xu, X. Zhou, J. Xiao, Q. Xia, Y. Li and Z. Li, *Chem. Eng. Sci.*, 2016, **148**, 275–281.
73 H. Zeng, X.-J. Xie, M. Xie, Y.-L. Huang, D. Luo, T. Wang, Y. Zhao, W. Lu and D. Li, *J. Am. Chem. Soc.*, 2019, **141**, 20390–20396.
74 D. Lv, J. Chen, Y. Chen, Z. Liu, Y. Xu, C. Duan, H. Wu, Y. Wu, J. Xiao, H. Xi, Z. Li and Q. Xia, *AIChE J.*, 2019, **65**, e16616.
75 J. Pires, J. Fernandes, K. Dedecker, J. R. B. Gomes, G. Pérez-Sánchez, F. Nouar, C. Serre and M. L. Pinto, *ACS Appl. Mater. Interfaces*, 2019, **11**, 27410–27421.
76 H. Wu, Y. Chen, W. Yang, D. Lv, Y. Yuan, Z. Qiao, H. Liang, Z. Li and Q. Xia, *Ind. Eng. Chem. Res.*, 2019, **58**, 10516–10523.
77 X. Wang, Z. Niu, A. M. Al-Enizi, A. Nafady, Y. Wu, B. Aguila, G. Verma, L. Wojtas, Y.-S. Chen, Z. Li and S. Ma, *J. Mater. Chem. A*, 2019, **7**, 13585–13590.
78 H. Wu, Y. Chen, D. Lv, R. Shi, Y. Chen, Z. Li and Q. Xia, *Sep. Purif. Technol.*, 2019, **212**, 51–56.
79 Y. Chen, H. Wu, D. Lv, R. Shi, Y. Chen, Q. Xia and Z. Li, *Ind. Eng. Chem. Res.*, 2018, **57**, 4063–4069.
80 D. Lv, R. Shi, Y. Chen, Y. Wu, H. Wu, H. Xi, Q. Xia and Z. Li, *ACS Appl. Mater. Interfaces*, 2018, **10**, 8366–8373.
81 Y. Chen, Z. Qiao, H. Wu, D. Lv, R. Shi, Q. Xia, J. Zhou and Z. Li, *Chem. Eng. Sci.*, 2018, **175**, 110–117.
82 W. Yuan, X. Zhang and L. Li, *J. Solid State Chem.*, 2017, **251**, 198–203.
83 P.-Q. Liao, W.-X. Zhang, J.-P. Zhang and X.-M. Chen, *Nat. Commun.*, 2015, **6**, 8697.
84 J. Pires, M. L. Pinto and V. K. Saini, *ACS Appl. Mater. Interfaces*, 2014, **6**, 12093–12099.
85 C. Gücüyener, J. van den Bergh, J. Gascon and F. Kapteijn, *J. Am. Chem. Soc.*, 2010, **132**, 17704–17706.
86 E. D. Bloch, L. J. Murray, W. L. Queen, S. Chavan, S. N. Maximoff, J. P. Bigi, R. Krishna, V. K. Peterson, F. Grandjean, G. J. Long, B. Smit, S. Bordiga, C. M. Brown and J. R. Long, *J. Am. Chem. Soc.*, 2011, **133**, 14814–14822.
87 H. Xiang, X. Fan and F. R. Siperstein, *Sep. Purif. Technol.*, 2020, **241**, 116635.
88 H. Tang and J. Jiang, *AIChE J.*, 2021, **67**, e17025.
89 C. He, Y. Wang, Y. Chen, X. Wang, J. Yang, L. Li and J. Li, *ACS Appl. Mater. Interfaces*, 2020, **12**, 52819–52825.
90 X. Zhang, J.-X. Wang, L. Li, J. Pei, R. Krishna, H. Wu, W. Zhou, G. Qian, B. Chen and B. Li, *Angew. Chem., Int. Ed.*, 2021, **60**, 10304–10310.
91 X. Zhang, L. Li, J.-X. Wang, H.-M. Wen, R. Krishna, H. Wu, W. Zhou, Z.-N. Chen, B. Li, G. Qian and B. Chen, *J. Am. Chem. Soc.*, 2020, **142**, 633–640.
92 K. Li, D. H. Olson, J. Seidel, T. J. Emge, H. Gong, H. Zeng and J. Li, *J. Am. Chem. Soc.*, 2009, **131**, 10368–10369.
93 C. Y. Lee, Y.-S. Bae, N. C. Jeong, O. K. Farha, A. A. Sarjeant, C. L. Stern, P. Nickias, R. Q. Snurr, J. T. Hupp and S. T. Nguyen, *J. Am. Chem. Soc.*, 2011, **133**, 5228–5231.
94 J. Peng, H. Wang, D. H. Olson, Z. Li and J. Li, *Chem. Commun.*, 2017, **53**, 9332–9335.
95 D.-X. Xue, A. Cadiau, Ł. J. Weseliński, H. Jiang, P. M. Bhatt, A. Shkurenko, L. Wojtas, C. Zhijie, Y. Belmabkhout, K. Adil and M. Eddaoudi, *Chem. Commun.*, 2018, **54**, 6404–6407.
96 L. Li, R.-B. Lin, X. Wang, W. Zhou, L. Jia, J. Li and B. Chen, *Chem. Eng. J.*, 2018, **354**, 977–982.
97 Y. Wang, N.-Y. Huang, X.-W. Zhang, H. He, R.-K. Huang, Z.-M. Ye, Y. Li, D.-D. Zhou, P.-Q. Liao, X.-M. Chen and J.-P. Zhang, *Angew. Chem., Int. Ed.*, 2019, **58**, 7692–7696.
98 H. Wu, Y. Yuan, Y. Chen, F. Xu, D. Lv, Y. Wu, Z. Li and Q. Xia, *AIChE J.*, 2020, **66**, e16858.
99 Q. Ding, Z. Zhang, C. Yu, P. Zhang, J. Wang, L. Kong, X. Cui, C.-H. He, S. Deng and H. Xing, *AIChE J.*, 2021, **67**, e17094.
100 R. Lyndon, W. You, Y. Ma, J. Bacsa, Y. Gong, E. E. Stangland, K. S. Walton, D. S. Sholl and R. P. Lively, *Chem. Mater.*, 2020, **32**, 3715–3722.
101 C. Gu, N. Hosono, J.-J. Zheng, Y. Sato, S. Kusaka, S. Sakaki and S. Kitagawa, *Science*, 2019, **363**, 387.
102 Q. Ding, Z. Zhang, C. Yu, P. Zhang, J. Wang, X. Cui, C.-H. He, S. Deng and H. Xing, *Sci. Adv.*, 2020, **6**, eaaz4322.
103 H. Wang, X. Dong, V. Colombo, Q. Wang, Y. Liu, W. Liu, X.-L. Wang, X.-Y. Huang, D. M. Proserpio, A. Sironi, Y. Han and J. Li, *Adv. Mater.*, 2018, **30**, 1805088.
104 B. Liang, X. Zhang, Y. Xie, R.-B. Lin, R. Krishna, H. Cui, Z. Li, Y. Shi, H. Wu, W. Zhou and B. Chen, *J. Am. Chem. Soc.*, 2020, **142**, 17795–17801.
105 Z. Bao, J. Wang, Z. Zhang, H. Xing, Q. Yang, Y. Yang, H. Wu, R. Krishna, W. Zhou, B. Chen and Q. Ren, *Angew. Chem., Int. Ed.*, 2018, **57**, 16020–16025.
106 C. Robl and A. Weiss, *Mater. Res. Bull.*, 1987, **22**, 373–380.
107 Y. Yang, L. Li, R.-B. Lin, Y. Ye, Z. Yao, L. Yang, F. Xiang, S. Chen, Z. Zhang, S. Xiang and B. Chen, *Nat. Chem.*, 2021, DOI: 10.1038/s41557-021-00740-z.

